1-1-1967

First order scattering of photons in spherical geometry

Ervin Thomas Boulette
Iowa State University

FIRST ORDER SCATTERING OF PHOTONS IN SPHERICAL GEOMETRY

by

Ervin Thomas Boulette

A Thesis Submitted to the
Graduate Faculty in Partial Fulfillment of
The Requirements for the Degree of
MASTER OF SCIENCE

Major Subject: Nuclear Engineering

Iowa State University
Of Science and Technology
Ames, Iowa

1967

TABLE OF CONTENTS

INTRODUCTION

Shortly after the discovery of X-rays it became apparent that there were possible harmful effects of these radiations. Ever since then, shielding against penetrating radiation has been a matter of concern and study.

With the advent of nuclear chain reactors, this problem of radiation shielding was magnified greatly. No longer was science dealing with the relatively low source strengths of radioactive materials, but now the intensities of available radioactive sources were increased many times. Consequently, larger and more effective shields had to be developed.

This increased importance of shielding has been responsible for extensive study of gamma radiation attenuation during the past decade. The attenuation of gamma radiation is of prime importance because of its characteristic nature. All types of radiation are present in the nuclear reactor; but the charged particles, by virtue of the electric charge, interact strongly with the atomic electrons of the matter through which they pass, and very quickly lose their energy. Thus it is the neutral particles, such as neutrons and gamma rays, that pose the major shielding problem.

The studies of the attenuation of neutrons and of gamma rays are very similar; however, in performing the calculations, the differing characteristics of each particle must be taken into account. In particular, a rather consequential

difference between gamma ray and neutron problems lies in the nature of the cross sections involved. Cross sections for gamma ray processes are smooth functions of both energy and atomic number. On the other hand, neutron cross section curves often exhibit resonance structure, in which both total cross section and angular distributions change drastically over narrow energy regions. Another dissimilarity between these two particles is due to the fact that the gamma ray dose is nearly proportional to the energy flux while the fast neutron dose is more nearly proportional to the number flux. Goldstein (6) and Fano, Spencer and Berger (4) consider further the details on the discrimination of these two problems.

The objective of this thesis is involved with the attenuation of gamma rays. Three methods have been extensively employed in calculating the attenuation of gamma radiation in matter. These are the method of successive scattering, the method of moments and the method of random sampling, more commonly called the Monte Carlo method. cursory description of the Monte Carlo technique and of the method of moments will be presented in this thesis. The method of successive scattering, however, will be presented in some detail, since it is the technique employed in this investigation.

The method of successive scattering has been successfully

applied to infinite-slab geometry by G. H. Peebles (13). This investigation is concentrated upon finite spherical geometry. Because of the inherent mathematical complications of this geometry, only first order scattering will be considered in this investigation. Number density ratios, as well as energy density ratios, of first order scattering to zero order scattering will be calculated for various materials, source energies, and dimensions.

LITERATURE REVIEW AND DISCUSSION OF THEORY

It is beyond the scope of this investigation to present an extended description of the various processes by which gamma rays interact with matter. The subject is treated in detail in a number of standard references and the present discussion is only an outline to supply a suitable background for the investigation. Among the numerous references on the fundamentals of gamma ray interaction processes are a large number of papers, reports and books. The latter include Segre (14), Friedlander and Kennedy (5), and Kaplan (9); all of whom present a rather straightforward approach. Other useful presentations have been given by Fano (3a,3b), White (17), Bethe and Ashkin (1), Goldstein and Wilkins (7), Goldstein (6), Snyder and Powell (15), and Davisson and Evans (2). Although somewhat more difficult, the classic reference for a basic understanding of the fundamental phenomena is the treatise by Heitler (8). Each contains an excellent presentation on gamma ray attenuation, covering all aspects of the problem and including considerable data.

The Interactions of Gamma Rays with Matter

Even upon restricting the energy range to the region of interest, from 100 kev to 4 Mev, there is a large variety of mechanisms by which photons can interact with matter. Table 1 lists these various modes of interactions in order of

relative importance for attenuation calculations in this energy range.

Table 1. Gamma ray interaction processes

A.	Primary
	1. Photoelectric effect
	2. Compton scattering
	3. Pair Production
B.	Secondary
	4. Coherent (Rayleigh) Electron scattering
	5. Annihilation radiation
	6. Fluorescence radiation
	7. Bremsstrahlung
	8. Thomson scattering from the nucleus
	9. Delbruck or Potential scattering
	10. Multiple Bragg scattering
	11. Nuclear interactions
	a. photoeffects
	b. scattering
	12. Radiative corrections to lower order processes

The various secondary processes listed in Table 1 are only of minute importance; therefore, no further discussion concerning these processes will be presented. This is particularly true in the energy range with which this

investigation is concerned. The three primary modes of interactions listed in Table 1, however, contribute overwhelmingly to the majority of photon interaction in this energy range, thus it is felt that a brief explanation of these modes should be presented.

Photoelectric effect

In the photoelectric effect, an incident photon transfers all of its energy to one of the atomic electrons which is then ejected from the atom. The energy of the emitted electron is equal to the incident photon energy less the ionization energy of the electron. Thus, this mode of interaction is characterized by the fact that it has a threshold energy; i.e., it can occur only when the energy of the incident photon is greater than the binding energy of the electron. However, for photon energies very large in comparison to the electron ionization energy, the photoelectric effect becomes relatively unimportant. Since the binding energy increases rapidly as Z increases, the photoelectric effect becomes more prominent for heavy elements. Heitler (8) states that this cross section is proportional to Z^5, while Goldstein (6) contends that it is between Z^4 and Z^5. Thus for the heavier elements the photoelectric effect predominates. In fact, for uranium it provides one-half the total absorption coefficient for photon energies up to 620 kev as indicated by Goldstein (6).

The important characteristic of this type of photon interaction is that the photon is absorbed, and thus does not contribute to the photon number density leaving the medium in which the interaction takes place. This is an important characteristic of this mode of interaction, and it will be considered further in the investigation.

Compton scattering

Whereas the photoelectric effect is an absorptive process, the Compton effect does not result in the destruction of the photon. Rather, the Compton effect is a scattering process which alters the direction and the energy of the incident photon. This is the source of the major difficulty in calculating gamma ray attenuation.

The Compton effect is the result of photons interacting with essentially free electrons. The photon collides with the free electron resulting in a scattered photon whose energy is equal to the energy of the incident photon less the kinetic energy of the scattered free electron. Kaplan (9) presents the standard treatment of Compton scattering and covers the main features quite adequately. This approach yields the following relationship for the energy $h\nu'$ of a scattered photon in terms of the incident photon energy $h\nu$ and the angle of scattering β:

$$h\nu' = \frac{h\nu}{1 + \frac{h\nu}{m_o c^2}(1-\cos\beta)} \quad . \qquad (1)$$

This relationship may be expressed in terms of wavelengths since $\lambda\nu = c$. Thus

$$\frac{1}{\lambda'} = \frac{\frac{1}{\lambda}}{1 + \frac{h}{\lambda m_o c}(1-\cos\beta)} , \tag{2}$$

or

$$\frac{\lambda' m_o c}{h} - \frac{\lambda m_o c}{h} = 1-\cos\beta . \tag{3}$$

These Compton relationships take particularly simple form if the photon wavelength λ and the energy, $h\nu = E$, are expressed in units of the Compton wavelength

$$h/m_o c = 0.02426 \text{ Å}$$

and the electron rest mass energy

$$m_o c^2 = 0.5110 \text{ Mev},$$

respectively. In these units, the relation between the change in photon wavelength and the angle of scattering is simply

$$\lambda'-\lambda = 1-\cos\beta. \tag{4}$$

Expressed in terms of energy Equation 4 appears as

$$E' = \frac{E}{1+E(1-\cos\beta)} . \tag{5}$$

In order to calculate the contribution of Compton scattering to the attenuation of photons, it is necessary to calculate the probability that such an occurrence will take place. This probability was derived on the basis of

relativistic quantum mechanics by Klein and Nishina and is covered quite thoroughly by Leipunskii, Novozhilov and Sakharov (11). The Klein Nishina formula for the total scattering cross section per electron is

$$\sigma_c(E) = \pi r_o^2 \{ \frac{E^2-2E-2}{E^3} \ln(1+2E) + 2 \frac{2+8E+9E^2+E^3}{E^2(1+2E)^2} \}. \qquad (6)$$

Besides the total cross section, it is also necessary to know the differential cross section for scattering; i.e., the cross section with respect to unit solid angle. This is expressed by the formula of Klein and Nishina

$$\frac{d\sigma_c}{d\Omega} = \frac{1}{2} r_o^2 (\frac{E'}{E})^2 [\frac{E'}{E} + \frac{E}{E'} + 2(\frac{1}{E} - \frac{1}{E'}) + (\frac{1}{E} - \frac{1}{E'})^2]$$

$$\delta(1 + \frac{1}{E} - \frac{1}{E'} - \cos\beta) , \qquad (7)$$

where r_o is the classical electron radius

$$r_o = 2.82 \times 10^{-13} \text{ cm.}$$

Equation 7 may also be expressed in terms of Compton wavelengths as

$$d\sigma_c = \frac{1}{2} r_o^2 (\frac{\lambda}{\lambda'})^2 [\frac{\lambda}{\lambda'} + \frac{\lambda'}{\lambda} + 2(\lambda-\lambda') + (\lambda-\lambda')^2]$$

$$\delta(1+\lambda-\lambda'-\cos\beta) d\Omega \ . \qquad (8)$$

The Dirac delta function, $\delta(1+\lambda-\lambda'-\cos\beta)$, has been introduced into Equation 8 in order to satisfy the condition expressed by Equation 4.

In the preceding discussion, it was shown that the

cross section per atom varied as Z. From the above equations, it can be seen that the total cross section is also dependent upon the incident photon energy. Data given by Goldstein (6) illustrate that Compton scattering predominates over the energy range being investigated. Even for an element as heavy as uranium, the Compton effect forms the major part of the total absorption coefficient from 0.6 to 5 Mev.

Pair production

In pair production all the energy of the incident photon is transformed into the creation of an electron pair, an electron and a positron. The total kinetic energy of the pair is equal to the energy of the incident photon less the rest mass of the pair; i.e., twice the rest mass of an electron. Pair production, therefore, has a threshold energy of $2m_oc^2$ or 1.022 Mev. Goldstein (6) presents a brief discussion of this phenomenon indicating the increasing effect of Z on the amount of pair production. For more details on this process of photon interaction, reference should be made to Kaplan (9), Leipunskii, Novozhilov and Sakharov (11) and Fano, Spencer and Berger (4).

Gamma Ray Absorption Coefficients

Consider a beam of incident photons of flux density I_o passing through an absorber of thickness x. The number of collisions made in a path length dx by photons passing in a

unit time through a unit cross sectional area of the beam is $I\sigma ndx$, where σ is the collision cross section and n is the number of atoms per unit volume. By substituting the absorption coefficient μ, equal to $n\sigma$, this value becomes $I\mu dx$. If these collisions are purely absorptive, this number of collisions must be exactly equal to the decrease in the flux density I over the distance dx

$$-dI = I\mu dx. \tag{9}$$

The solution to this differential equation is Lambert's law

$$I_x = I_o \exp(-\mu x). \tag{10}$$

From the considerations of the preceding section, the total photon cross section to be used in attenuation calculations is given by the sum of the cross sections for the photoelectric effect, Compton scattering and pair production:

$$\sigma_T = \sigma_{pe} + \sigma_c + \sigma_{pp} . \tag{11}$$

This total cross section is usually described as the mass absorption coefficient μ, and is expressed in units of cm^2/gm. Numerous tables of absorption coefficients are in existence based in varying proportions on calculations and measurements in narrow beam geometry. Probably the most important of these are those compiled by Snyder and Powell (15), Latter and Kahn (10) and G. R. White (17). The latter is the more recent and is believed to contain values accurate to within two per cent. For the purpose of this investigation total linear absorption coefficients μ_T were used.

The data source employed for these various attenuation coefficients is U.S. Atomic Energy Commission (16).

Methods of Calculating Gamma Ray Attenuation

The well known Boltzmann transport equation is satisfied by the distribution function for gamma rays. The transport equation is simply the balance of photons in six-dimensional phase space ($\bar{r}$, $\bar{\Omega}$, E). In the stationary case, the number of photons in the element of phase space volume dV = $d\bar{r}d\bar{\Omega}dE$ should remain constant. The most straight forward approach to the derivation of the transport equation is to consider the various processes by which photons enter and leave the element of phase space volume dV.

First of all, it is necessary to consider the migration of quanta from an element of volume of ordinary space $d\bar{r}$, due to their motion. The flux through a unit area, the normal of which lies in the direction of $\bar{\Omega}$, is expressed by $N(\bar{r}, \bar{\Omega}, E)d\bar{\Omega}dE$; thus the variation in the number of photons in unit time in the volume dV as a result of their free motion has the form

$$\text{div}\,[\bar{\Omega}N(\bar{r}, \bar{\Omega}, E)]\, d\bar{r}d\bar{\Omega}dE \,. \qquad (12)$$

Photons may disappear from this volume element of phase space by absorptive interactions with matter. The loss of photons in dV per unit time due to this process is

$$\mu(E)N(\bar{r}, \bar{\Omega}, E)d\bar{r}d\bar{\Omega}dE \,, \qquad (13)$$

where $\mu(E)$ is the linear absorption coefficient.

The volume element $d\bar{r}$ may contain a source of photons with energy E and direction of motion along $\bar{\Omega}$. Thus in the equation of balance, a term must be introduced to take into account the photons born within the phase space volume element in unit time from the source:

$$S(\bar{r},\bar{\Omega},E)d\bar{r}d\bar{\Omega}dE , \tag{14}$$

where $S(\bar{r},\bar{\Omega},E)$ is defined as the number of photons emitted by the source in unit time in a unit volume around the point determined by the radius vector $\bar{r}$ in a unit energy interval around the energy E and in a unit solid angle around the direction of $\bar{\Omega}$.

Finally, photons from the phase space volume element $dV' = d\bar{r}d\bar{\Omega}'dE'$ may be scattered, by the Compton effect, into the phase space volume element $dV = d\bar{r}d\bar{\Omega}dE$. The energy of these photons changes from E' to E and the direction of motion, from $\bar{\Omega}'$ to $\bar{\Omega}$. This transition of photons from dV' to dV is expressed as

$$n_o\sigma(\bar{\Omega}'\rightarrow\bar{\Omega},E'\rightarrow E)d\bar{\Omega}dEN(\bar{r},\bar{\Omega}',E')d\bar{\Omega}'dE'd\bar{r}', \tag{15}$$

where $\sigma(\bar{\Omega}'\rightarrow\bar{\Omega},E'\rightarrow E)$ is the differential cross section for the transition of photons from the state $(\bar{r},\bar{\Omega}',E')$ to the state $(\bar{r},\bar{\Omega},E)$ and n_o is the number of electrons in unit volume. The total number of photons arriving at dV as a result of Compton scattering is thus

$$n_o d\bar{r} d\overline{\Omega}\, dE \int_{4\pi} d\overline{\Omega}' \int_{E}^{\infty} dE' \sigma(\overline{\Omega}' \rightarrow \overline{\Omega}, E' \rightarrow E) N(\bar{r}, \overline{\Omega}', E') . \quad (16)$$

In the stationary state, the number of photons leaving the volume element dV equals the number of photons entering this volume element. Thus the sum of Equations 14 and 16 must equal the sum of Equations 12 and 13. Dividing all terms by dV, one obtains the transport equation

$$\begin{aligned} \mathrm{div}[\,\overline{\Omega} N(\bar{r}, \overline{\Omega}, E)\,] + \mu(E) N(\bar{r}, \overline{\Omega}, E) \\ = n_o \int_{4\pi} d\overline{\Omega}' \int_{E}^{\infty} dE' \sigma(\overline{\Omega}' \rightarrow \overline{\Omega}, E' \rightarrow E) N(\bar{r}, \overline{\Omega}', E') \\ + S(\bar{r}, \overline{\Omega}, E) . \end{aligned} \quad (17)$$

Equation 17 is the most general form of the Boltzmann transport equation for photons. Further modifications in the form of the equation depend upon the source and medium geometry. Leipunskii, Novozhilov and Sakharov (11) investigate a variety of source types and scattering medium geometries.

A direct solution to the integro-differential transport equation has been under severe investigation for the past three decades; however, no "quick and dirty" method of solving this equation has been found as of yet.

A direct numerical integration of the time independent Boltzmann transport equation has been attempted; however, it requires integration over at least six variables

(e.g., $\bar{r}$,E,$\overline{\Omega}$) and threatens to tax the capabilities even of the largest electronic computers. However, in the course of much investigation, three numerical techniques have been developed which approximate solutions to the transport equation. These techniques are the method of moments, the Monte Carlo method and the method of successive scattering. The highlights of the method of moments and of the Monte Carlo method will be discussed only briefly since they are not involved in this investigation. For further details, one should refer to Leipunskii, Novozhilov and Sakharov (11), Fano, Spencer and Berger (4) and Goldstein (6).

The method of moments

Most of the theoretical results for multiple scattering of photons have been obtained by employing the method of moments to generate a numerical solution to the transport equation. The principal results of the calculations are given by Goldstein and Wilkins (7).

It should be noted that this numerical technique employed for the solution of the transport equation is applicable only to infinite homogeneous media and simple types of geometry for the source.

Essentially, the method of moments is based on the fact that the integro-differential transport equation for the gamma ray distribution function may be transformed into a system of coupled integral equations for the space-angle

moments of the distribution function. A numerical solution of the system of equations can be obtained with the aid of an electronic computer and the moments so derived are used to reconstruct the gamma ray distribution function.

The Monte Carlo method

Unlike the method of moments, the Monte Carlo method may be applied to problems with any kind of geometry, including cases of propogation of photons through finite media. For this reason, the main results of the determination of the transmission coefficients of photons through slabs and the reflexion coefficients (albedo) from various media have been obtained by this particular method.

The essence of the Monte Carlo method lies in the fact that the complex statistical process of the transmission of a photon through matter may be considered as a succession of a finite number of random elementary processes (e.g., free motion over a certain path, disappearance through pair production or photoelectric effect, Compton scattering in a definite direction, etc.). If the probability of each of these occurrences is determined and a list of random numbers is available, the trajectory of a particular photon in the medium under investigation may be reproduced step by step. On reaching the stage at which the photon disappears or is transferred to a state in which one is interested (e.g., the photon crosses the boundary of the scattering medium) the

trajectory of the next photon is investigated. If a sufficiently large number of photon trajectories are investigated in this manner, a photon distribution function according to energy, angle or some other variable may be finally obtained.

The difficulties arising from the Monte Carlo application to the solution of the Boltzmann transport equation lie in the expressions given for probable errors. To minimize the probable error, one must generate an extremely large number of photon trajectories. Goldstein (6) states that for penetrations of 10^{-6}, the starting sample of photon trajectories would have to be of order of 10^{8} to 10^{9}, requiring many hours of computer time. To resolve this dilemma, different types of artificial methods have been worked out by which the number of trajectories may be reduced without increasing the probable error.

Although the Monte Carlo method involves large amounts of computer time, its value is nevertheless without question. In particular, it seems to be one of the few practical means known for solving problems involving multiple layers, the present outstanding gap in shielding theory.

The method of successive scattering

The method of successive scattering has been successfully applied to the case of infinite slab geometry by Peebles (13). The principle involved is relatively simple and will be described in detail.

The probability that a photon will be transmitted through a slab of finite thickness but infinite extent is the sum of the probabilities that it will be transmitted with no scattering, with one scattering, with two scattering, etc. Generally, the first few scatterings are sufficient for accurate determinations of total transmission if the slab in question is thin; however, if the slab is thick, an excessive number of scatterings is required for great accuracy.

The probability that a photon will be transmitted through a slab with exactly k collisions may be expressed as the product of four probabilities: (1) $\exp(-\mu_o a)$, the probability that the photon will travel a distance a in the material without interaction, where μ_o is the total linear absorption coefficient of the source energy; (2) $\mu_o da$, the probability that an interaction will take place in da at a; (3) $\rho d\sigma/\mu_o$, the probability that the photon will survive that collision and scatter into a new path, where ρ is the electron density and $d\sigma$ is the Klein Nishina differential cross section per electron; and (4) N_{k-1}, the probability that the photon will continue through the slab suffering exactly k-1 collisions before its emergence from the slab. Thus, for small values of k, one can write

$$dN_k = \exp(-\mu_o a) \cdot \mu_o da \cdot \rho d\sigma/\mu_o \cdot N_{k-1}, \qquad (18)$$

where N_k is defined as the probability that the photon will be transmitted through the slab with exactly k collisions.

The diagram illustrated in Figure 1 serves to clarify the derivation of this equation.

The probability that a photon will be transmitted without suffering an interaction is

$$N_o = \exp(-X/\gamma_o), \tag{19}$$

where X is the slab thickness in mean free paths (calculated at the incident energy) and γ_o is the cosine of the angle between the normal to the slab and the incident path. Equation 19, in conjunction with Equation 18, yields N_1, the probability that the photon suffers exactly one collision as it is transmitted through the slab. Iteration of this technique yields values for N_2, N_3, N_4, etc. Obviously, this technique involves a considerable amount of work, since at each step, N_{k-1} must be known for a sufficiently wide range of three parameters--slab thickness, incident energy and incident angle. However, the considerable amount of generated information justifies the large amount of time involved in using this numerical technique.

The application of similar arguments may be employed to generate values for E_k, the expected energy transmitted in the beam after exactly k collisions. The equation for E_k is very similar to that for N_k, in particular

$$dE_k = \exp(-\mu_o a)\cdot\mu_o da\cdot\rho d\sigma/\mu_o\cdot E_{k-1} \ . \tag{20}$$

Peebles (13) has generated much data employing this technique. He has calculated values of N_k/N_o and E_k/E_o for

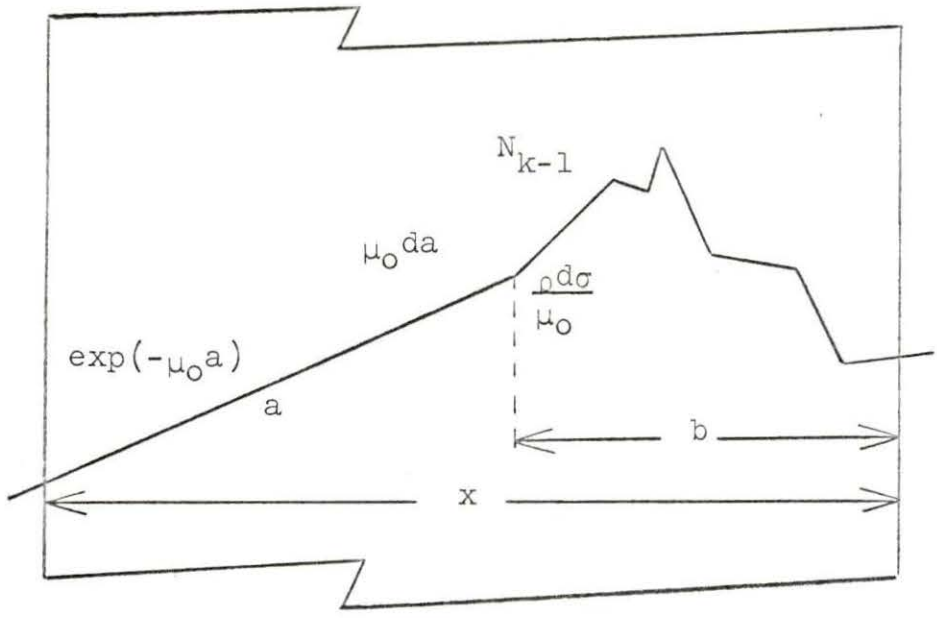

Figure 1. A diagram showing the probabilities associated with the transmission of a photon and clarifying the derivation of Equation 18.

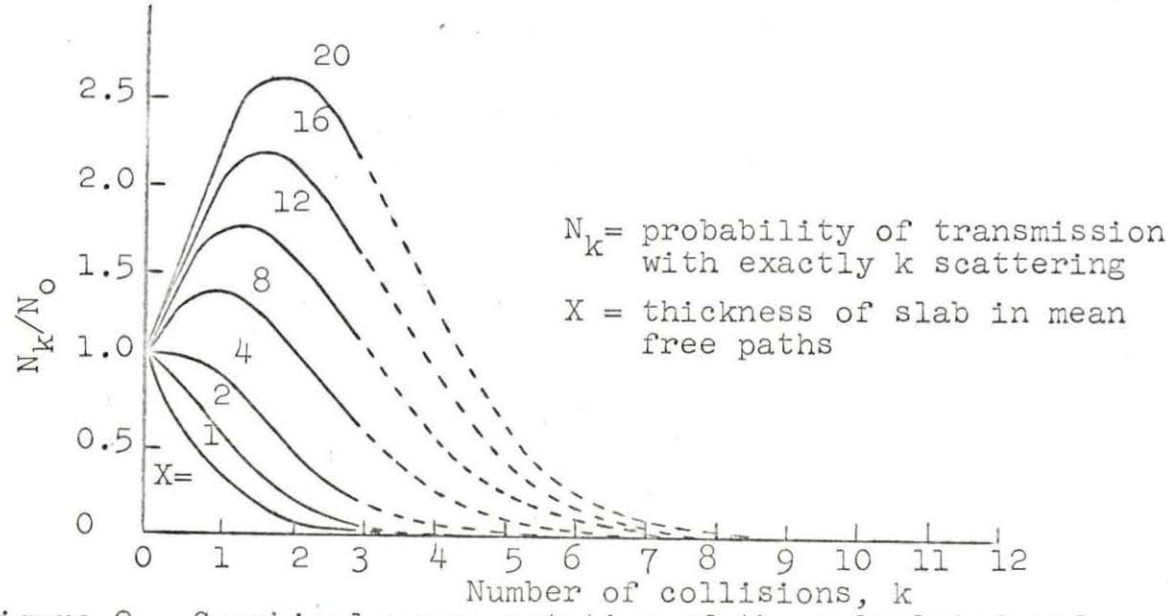

Figure 2. Graphical representation of the calculated and estimated behavior of N_k/N_o with respect to k in the case of a photon of energy 5 $m_o c^2$ normally incident on a lead slab.

infinite lead and iron slabs of various thicknesses and for various source strengths and incident path angles. Although this investigation is limited to first order scattering only, Peebles has performed calculations for first, second and third order scatterings. His results have been reproduced in a graphical manner in Figure 2.

FIRST ORDER SUCCESSIVE SCATTERING METHOD APPLIED TO SPHERICAL GEOMETRY

The equations generated by the application of the successive scattering technique take different forms for different properties of the system. Thus before attempting to derive the necessary equations for attenuation calculations, the physical properties of the system must be defined.

This investigation is concerned with the derivation of formulas yielding N_1 and E_1 for a monoenergetic, isotropic point source in finite spherical geometry. Only first order scattering will be considered.

Probabilities Expressed in Spherical Geometry

In an analogous manner to Peebles' treatment of the infinite slab case, the derivation of dN_1 and dE_1 will result from the product of four probabilities. Figure 3 serves to define the variables involved in this problem as well as to indicate a typical path of a first order scattered photon.

The probability P_1 that a photon emitted from the source will travel a distance a before interacting in the sphere is

$$P_1 = \frac{\exp(-\mu_o a) a^2 \sin\theta d\theta d\varphi}{4\pi a^2} . \qquad (21)$$

P_2 is defined as the probability that the photon will suffer a collision in da at a distance a from the source. The form of this probability is

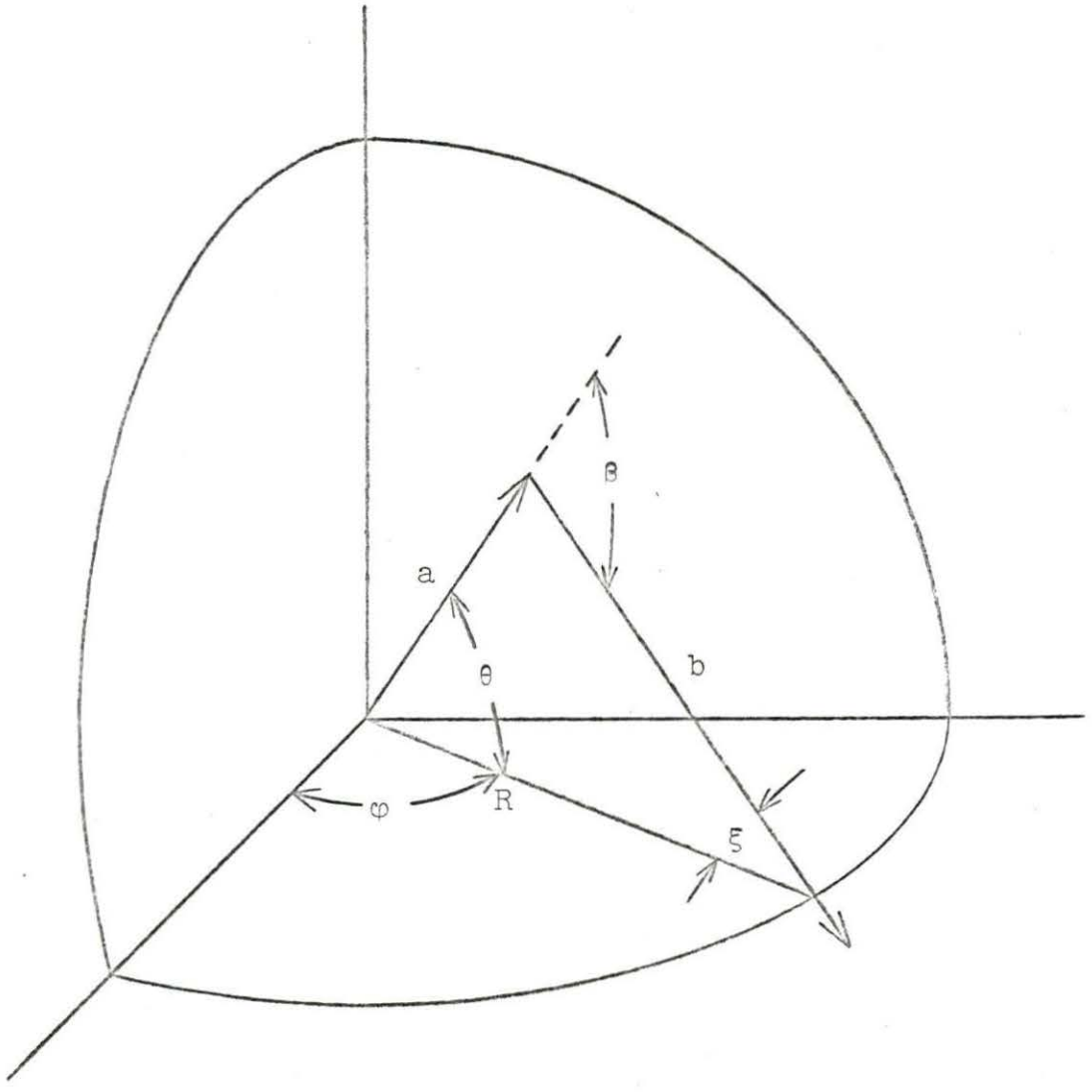

Figure 3. The path of a photon suffering a scattering collision at a and scattered by angle β.

$$P_2 = \mu_o da \ . \tag{22}$$

The probability P_3 that the photon survives the collision and is scattered into a scattering angle β is expressed as

$$P_3 = \rho d\sigma/\mu_o \ , \tag{23}$$

where ρ is the electron density and $d\sigma$ is the Klein Nishina differential cross section. From Equation 8

$$d\sigma = \frac{1}{2} r_o^2 \left(\frac{\lambda}{\lambda'}\right)^2 \left[\frac{\lambda}{\lambda'} + \frac{\lambda'}{\lambda} + 2(\lambda-\lambda') + (\lambda-\lambda')^2\right] \delta(1+\lambda-\lambda'-\cos\beta) d\Omega, \tag{24}$$

where $d\Omega$ is an element of unit solid angle. For simplification, $\varkappa(\lambda,\lambda')$ is defined as

$$\varkappa(\lambda,\lambda') = \frac{1}{2} r_o^2 \left(\frac{\lambda}{\lambda'}\right)^2 \left[\frac{\lambda}{\lambda'} + \frac{\lambda'}{\lambda} + 2(\lambda-\lambda') + (\lambda-\lambda')^2\right]; \tag{25}$$

thus P_3 becomes

$$P_3 = \frac{\rho \varkappa(\lambda,\lambda') \delta(1+\lambda-\lambda'-\cos\beta) d\Omega}{\mu_o} \ . \tag{26}$$

Finally, the probability that the photon will continue from the point of collision to the surface of the sphere is

$$P_4 = \exp(-\mu b) \ , \tag{27}$$

where μ is the attenuation coefficient of the scattered photon, and b is the distance from the point of scattering to the surface of the sphere.

The product of P_1, P_2, P_3, and P_4 yields the desired expressions for dN_1

$$dN_1 = \frac{\exp(-\mu_o a)a^2 \sin\theta d\theta d\varphi}{4\pi a^2} \cdot \mu_o da \cdot \frac{\rho_\kappa(\lambda,\lambda')\delta(1+\lambda-\lambda'-\cos\beta)d\Omega}{\mu_o}$$

$$\cdot \exp(-\mu b) \ . \qquad (28)$$

Integration of this equation yields the following expression for N_1:

$$N_1 = \int_{\substack{\text{total}\\ \text{solid}\\ \text{angle}}} d\Omega \int_0^{2\pi} d\varphi \int_0^{\pi} d\theta \int_0^{R} da \left[\frac{\exp(-\mu_o a)\sin\theta}{4\pi} \cdot \rho_\kappa(\lambda,\lambda')\right.$$

$$\left. \delta(1+\lambda-\lambda'-\cos\beta)\cdot \exp(-\mu b)\right]. \qquad (29)$$

The variable φ, by nature of the geometry of the problem, may be eliminated by integrating directly over φ; thus

$$N_1 = \int_{\substack{\text{total}\\ \text{solid}\\ \text{angle}}} d\Omega \int_0^{\pi} d\theta \int_0^{R} da\left[\frac{1}{2} \exp(-\mu_o a)\cdot \rho_\kappa(\lambda,\lambda')\delta(1+\lambda-\lambda'-\cos\beta)\right.$$

$$\left. \cdot \exp(-\mu b)\right] \ . \qquad (30)$$

The variable θ may be eliminated by considering Figure 3 and employing the sine law. Thus

$$\theta = \beta - \xi \qquad (31)$$

and

$$\xi = \arcsin\left[\frac{a}{R} \sin(\pi-\beta)\right] = \arcsin\left[\frac{a}{R} \sin\beta\right]; \qquad (32)$$

therefore,

$$\theta = \beta - \arcsin\left[\frac{a}{R} \sin\beta\right] \ . \qquad (33)$$

The relationship between $d\theta$ and $d\beta$ is not quite as easily acquired; however, an investigation of Figure 4 will help clarify the problem. From the definition of the sine of an

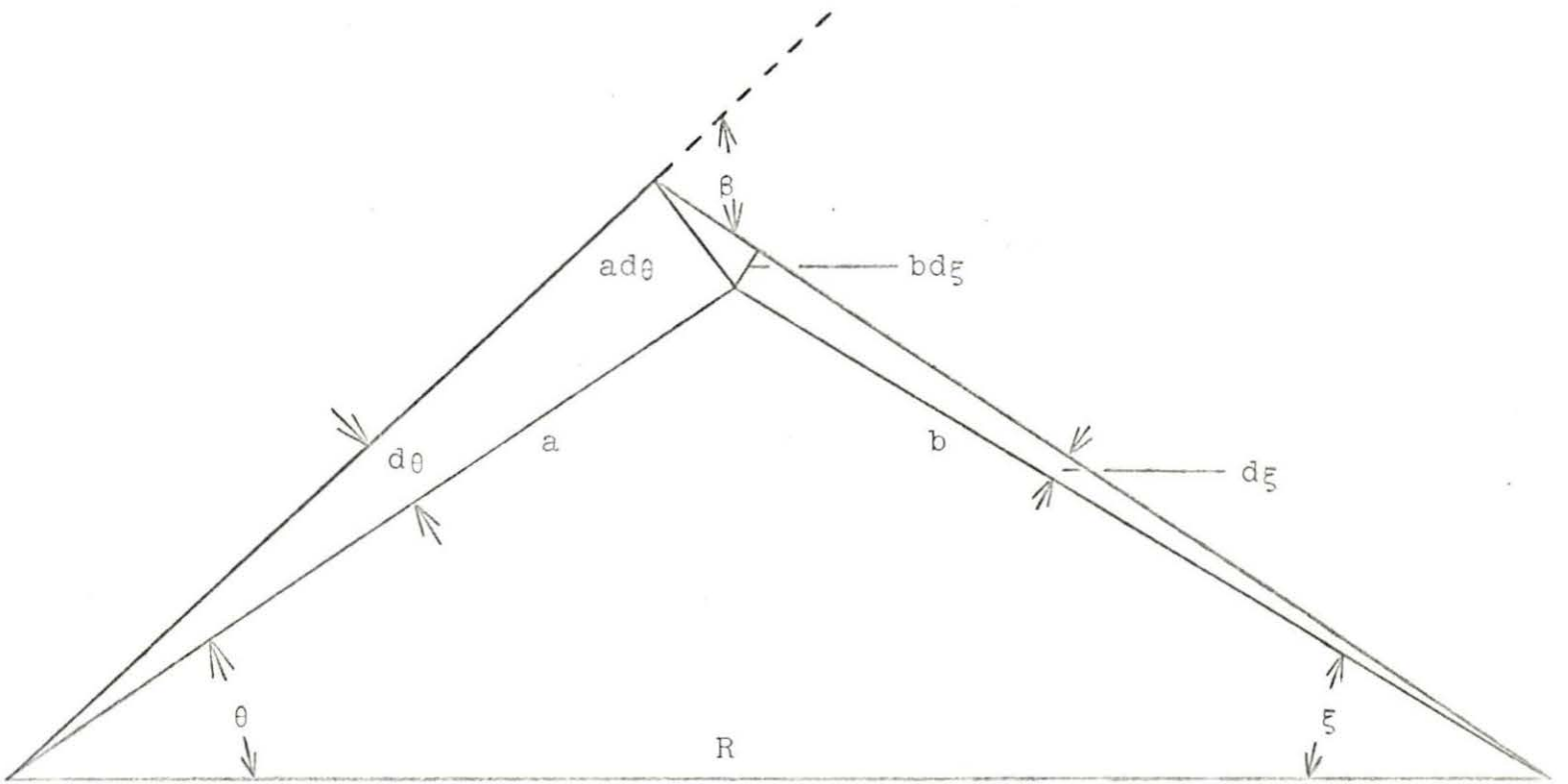

Figure 4. The relationship between $d\theta$ and $d\beta$.

angle, the following relationship is derived:

$$\frac{b\,d\xi}{a\,d\theta} = \sin\left(\frac{\pi}{2} - \beta\right) = \cos\beta \ , \tag{34}$$

or

$$d\xi = \frac{a}{b}\cos\beta \, d\theta \ . \tag{35}$$

Differentiation of Equation 31 yields

$$d\theta = \frac{\partial\theta}{\partial\beta} d\beta + \frac{\partial\theta}{\partial\xi} d\xi = d\beta - d\xi \tag{36}$$

since $\partial\theta/\partial\beta$ and $-\partial\theta/\partial\xi$ equal one. Thus

$$d\theta = d\beta - \frac{a}{b}\cos\beta \, d\theta \ , \tag{37}$$

or, after appropriate simplifications have been performed

$$d\theta = \frac{b\,d\beta}{b + a\cos\beta} \ . \tag{38}$$

Now consider the variable $\overline{\Omega}$. As is seen in Figure 5,

$$\int_{\substack{\text{total}\\\text{solid}\\\text{angle}}} d\Omega = \int_0^{2\pi} d\varphi' \int_0^{\pi} \sin\beta d\beta \ . \tag{39}$$

As in the treatment of the φ variable, φ' may be directly integrated because of the symmetry of the problem. Thus

$$\int_{\substack{\text{total}\\\text{solid}\\\text{angle}}} d\Omega = 2\pi \int_0^{\pi} \sin\beta d\beta \ . \tag{40}$$

Consider at this point the Compton relationship between the scattered photon wavelength λ' and the angle of scattering β, expressed by Equation 4. By differentiating this equation,

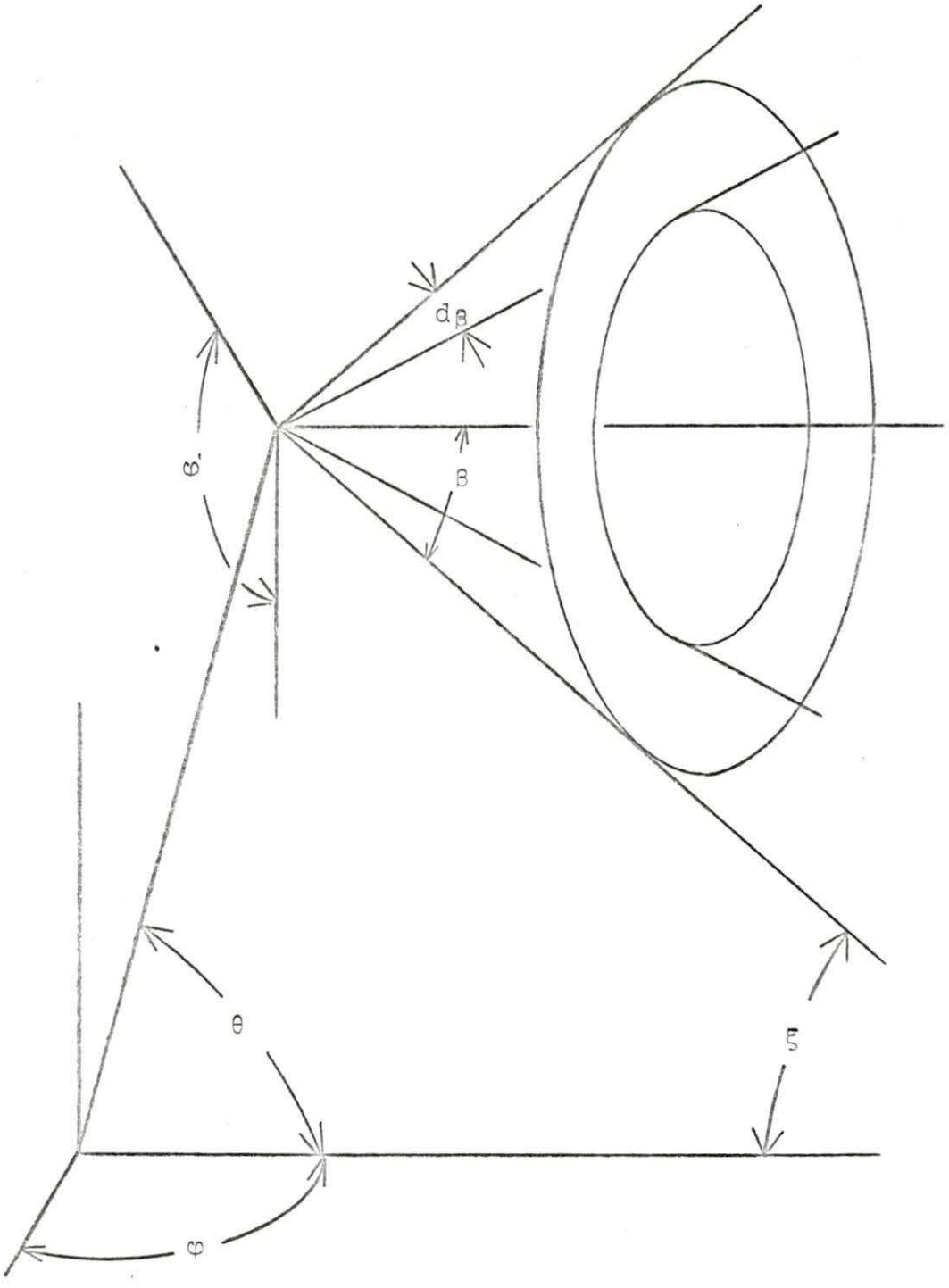

Figure 5. The relationship between $d\Omega$ and $d\lambda'$.

one obtains

$$d\lambda' = \sin\beta d\beta \ . \tag{41}$$

The substitution of Equation 41 into Equation 40 yields a relationship between $d\Omega$ and $d\lambda'$; in particular,

$$\int_{\substack{\text{total}\\\text{solid}\\\text{angle}}} d\Omega = 2\pi \int_{\lambda}^{\lambda+2} d\lambda' \ , \tag{42}$$

where the limits of integration over the λ' variable have been derived from Equation 4.

The substitution of Equations 42, 38 and 33 into Equation 30 yields the following expression for N_1:

$$N_1 = \int_{\lambda}^{\lambda+2} d\lambda' \int_{0}^{\pi} d\beta \int_{0}^{R} da\Big[\pi \exp(-\mu_o a)\cdot \sin\{\beta - \arcsin(\tfrac{a}{R}\sin\beta)\}$$

$$\cdot \rho_{\kappa}(\lambda,\lambda')\delta(1+\lambda-\lambda'-\cos\beta)\cdot \exp(-\mu b)\cdot \frac{b}{b+a\cos\beta}\Big]. \tag{43}$$

As Equation 43 indicates, N_1 is expressed in terms of four variables--a, b, λ', and β. The variable b may be eliminated quite easily by application of the sine law; i.e.,

$$\frac{b}{\sin\theta} = \frac{R}{\sin(\pi-\beta)} \tag{44}$$

The substitution of Equation 33 into Equation 44 and simplification of the resulting equation yields the following relationship between b, a and β:

$$b = R\Big[\cos\{\arcsin(\tfrac{a}{R}\sin\beta)\} - \frac{a}{R}\cos\beta\Big] \ . \tag{45}$$

Now consider the variable β and the Dirac delta function $\delta(1+\lambda-\lambda'-\cos\beta)$. If a function $f(x,y,z)$ exists such that

$$f(x,y,z) = \int dx \int dy \int dz \{g(x,y,z)\delta[h(x,y,z)]\} \quad (46)$$

then an equivalent expression for $f(x,y,z)$ is

$$f(x,y,z) = \int dx \int dy \left\{\frac{g(x,y,z)}{|\partial h/\partial z|}\right\}, \quad (47)$$

where $g(x,y,z)$ and $\partial h/\partial z$ are evaluated at z such that $h(x,y,z)$ equals zero. The application of this property of the Dirac delta function to Equation 43 results in the elimination of the β variable. The form of the function h in Equation 43 is

$$h(\lambda',\beta) = 1+\lambda-\lambda'-\cos\beta \quad (48)$$

thus

$$\partial h/\partial\beta = \sin\beta, \quad (49)$$

and setting Equation 48 equal to zero yields

$$\beta = \arccos(\lambda+1-\lambda'). \quad (50)$$

The application of the Dirac delta function property and the substitution of Equation 45 into Equation 43 yield an expression for N_1 in terms of only two variables, a and λ'. In particular, the equation for N_1 is

$$N_1 = \int_{\lambda}^{\lambda+2} d\lambda' \int_{0}^{R} da\ \pi \exp(-\mu_o a)\cdot\sin[\beta-\arcsin(\tfrac{a}{R}\sin\beta)]\cdot\rho_K(\lambda,\lambda')\cdot$$
$$\exp[-\mu R(\cos(\arcsin(\tfrac{a}{R}\sin\beta))-\tfrac{a}{R}\cos\beta)]\cdot\frac{R[\cos(\arcsin(\frac{a}{R}\sin\beta))-\frac{a}{R}\cos\beta]}{R[\cos(\arcsin(\frac{a}{R}\sin\beta))]\cdot|\sin\beta|}, \quad (51)$$

where $\beta = \arccos(1+\lambda-\lambda')$. Simplification of Equation 51 yields

$$N_1 = \int_{\lambda}^{\lambda+2} d\lambda' \int_{0}^{R} da\ \pi \exp -(\mu_o a+\mu R[\cos(\arcsin(\tfrac{a}{R}\sin\beta))-\tfrac{a}{R}\cos\beta]) \cdot \rho_{\mathcal{H}}(\lambda,\lambda') \cdot \frac{\{\cos[\arcsin(\frac{a}{R}\sin\beta)]-\frac{a}{R}\cos\beta\}^2}{\cos\{\arcsin(\frac{a}{R}\sin\beta)\}} \quad , \qquad (52)$$

where $\beta = \arccos(1+\lambda-\lambda')$.

E_1 equals the product of the energy of the scattered photon E' and the number density N_1 of the scattered photon. Since the units employed are the Compton unit of wavelength and the electron rest mass energy unit of energy, E' is the reciprocal of λ'. Thus the form of E_1 is

$$E_1 = \int_{\lambda}^{\lambda+2} d\lambda' \int_{0}^{R} da\ \frac{\pi}{\lambda'} \exp -(\mu_o a+\mu R[\cos(\arcsin(\tfrac{a}{R}\sin\beta))-\tfrac{a}{R}\cos\beta]) \cdot \rho_{\mathcal{H}}(\lambda,\lambda') \cdot \frac{\{\cos[\arcsin(\frac{a}{R}\sin\beta)]-\frac{a}{R}\cos\beta\}^2}{\cos\{\arcsin(\frac{a}{R}\sin\beta)\}} \quad . \qquad (53)$$

Numerical Integration

The analytical integration of Equations 52 and 53 would prove to be extremely difficult if not impossible. Therefore, for the purpose of this investigation, a numerical integration technique was employed. In particular recourse was made to Simpson's rule treated quite adequately by Wylie (18).

Simpson's rule for a single integral equation may be

expressed as

$$\int_{x_j}^{x_{j+2}} dx f(x) = \frac{h_x}{3} [f_j + 4f_{j+1} + f_{j+2}] , \qquad (54)$$

where $f_j = f(x_j)$, $f_{j+1} = f(x_{j+1})$ and $f_{j+2} = f(x_{j+2})$, and h_x is the distance between two adjacent points on the x-axis. In the case of a double integral equation, Simpson's rule is applied over both variables; i.e.,

$$\int_{x_j}^{x_{j+2}} dx \int_{y_k}^{y_{k+2}} dy\ f(x,y) = \int_{x_j}^{x_{j+2}} \{\frac{h_y}{3} [f_k + 4f_{k+1} + f_{k+2}]\},$$

or

$$\int_{x_j}^{x_{j+2}} dx \int_{y_k}^{y_{k+2}} dy\ f(x,y) = \frac{h_x h_y}{9} \{f_{k,j} + 4f_{k,j+1} + f_{k,j+2} + 4f_{k+1,j} + 16f_{k+1,j+1} + 4f_{k+1,j+2} + f_{k+2,j} + 4f_{k+2,j+1} + f_{k+2,j+2}\}. \qquad (55)$$

A better comprehension of the numerical integration technique employed is acquired by considering Figure 6.

Generally speaking, the smaller the values of h_x and h_y, the greater the accuracy of the approximation. However, when applying this technique, one must consider the amount of computer time required as well as the accuracy desired. If one is integrating over a relatively large region; i.e., the grid contains a large number of points, and the numerical solution indicates signs of convergence, one may adopt a criterion for the selection of the values of h_x and

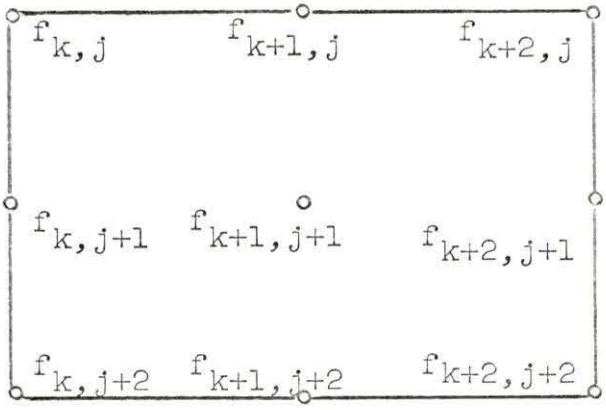

Figure 6. Simpson's rule applied to double integration.

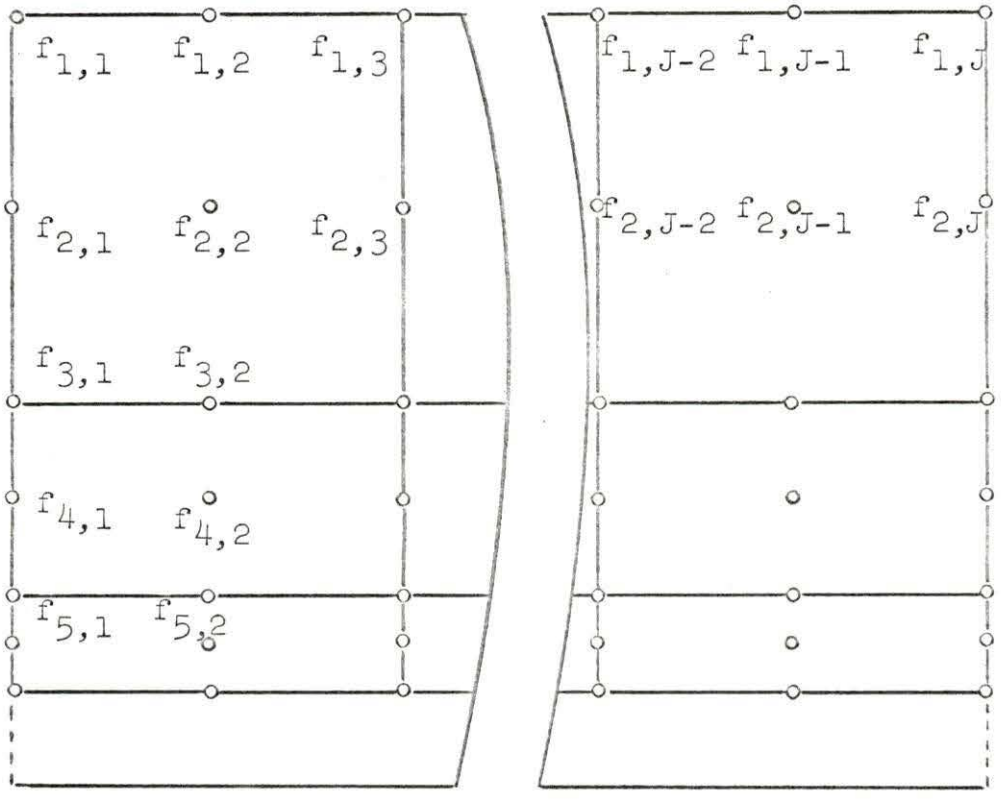

Figure 7. Iterated double integration Simpson's rule.

h_y by considering the trend of convergence. For instance, the value of h_x may be halved repeatedly until it appears that the solution has converged and that further halving of h_x contributes a negligible amount to the solution. Once this has been done for h_x, the procedure is then repeated for h_y.

Should the range of integration be such as to include more than three points along each of the variable axes, Simpson's rule is merely repeated in the following manner

$$\int_{x_1}^{x_n}\int_{y_1}^{y_n} f(x,y)\,dy\,dx = \int_{x_1}^{x_3}\int_{y_1}^{y_n} f(x,y)\,dy\,dx + \int_{x_3}^{x_5}\int_{y_1}^{y_n} f(x,y)\,dy\,dx + \cdots + \int_{x_{n-2}}^{x_n}\int_{y_1}^{y_n} f(x,y)\,dy\,dx, \tag{56}$$

and

$$\begin{aligned}\int_{x_1}^{x_n}\int_{y_1}^{y_n} f(x,y)\,dy\,dx = {} & \int_{x_1}^{x_3}\int_{y_1}^{y_3} f(x,y)\,dy\,dx + \int_{x_1}^{x_3}\int_{y_3}^{y_5} f(x,y)\,dy\,dx + \cdots \\ & + \int_{x_1}^{x_3}\int_{y_{n-2}}^{y_n} f(x,y)\,dy\,dx + \int_{x_3}^{x_5}\int_{y_1}^{y_3} f(x,y)\,dy\,dx + \int_{x_3}^{x_5}\int_{y_3}^{y_5} f(x,y)\,dy\,dx + \cdots \\ & \cdots + \int_{x_3}^{x_5}\int_{y_{n-2}}^{y_n} f(x,y)\,dy\,dx + \cdots + \int_{x_{n-2}}^{x_n}\int_{y_1}^{y_3} f(x,y)\,dy\,dx \\ & + \int_{y_{n-2}}^{x_n}\int_{y_3}^{y_5} f(x,y)\,dy\,dx + \cdots + \int_{x_{n-2}}^{x_n}\int_{y_{n-2}}^{y_n} f(x,y)\,dy\,dx.\end{aligned} \tag{57}$$

The application of Simpson's rule to each of the double integral terms on the right hand side of Equation 57 then yields

$$\int_{x_1}^{x_n}\int_{y_1}^{y_n} f(x,y)\,dy\,dx = \frac{h_x h_y}{9}\left[f_{1,1} + \sum_{j=3,5,7,\ldots}^{J}\sum_{k=3,5,7,\ldots}^{K} [2(f_{k,1}+f_{1,j})+4f_{k,j}] + \sum_{j=2,4,6,\ldots}^{J-1}\sum_{k=2,4,6,\ldots}^{K-1} [4(f_{1,j}+f_{k,1})+16f_{k,j}] + \sum_{k=2,4,6,\ldots}^{K-1}\sum_{j=3,5,7,\ldots}^{J} 8f_{k,j} + \sum_{k=3,5,7,\ldots}^{K}\sum_{j=2,4,6,\ldots}^{J-1} 8f_{k,j} \right] . \qquad (58)$$

The application of this numerical technique to N_1 and E_1 resulted in the grid illustrated in Figure 7. It was decided that the criterion for the most appropriate choice of values for $h_{\lambda'}$ and h_a should be that the change in the numerical solution for N_1 for any value of h_a and $h_{\lambda'}$ be less than one per cent of the value of N_1 calculated for the preceding values of h_a and $h_{\lambda'}$.

The initial value of h_a was defined as the radius of the sphere in mean free paths divided by 40.0. This choice of h_a was completely arbitrary but as further investigation showed this was a proper choice since further division of h_a was entirely unnecessary. The value of $h_{\lambda'}$, however,

created somewhat of a problem. It was intuitively obvious that the contribution of backscattering to N_1 would be almost negligible. Also, it was expected that the major contribution to N_1 would result from scattering angles of the order of zero degrees. Thus, the value of $h_{\lambda'}$ should be quite small in the neighborhood of $\beta = 0$, but for β greater than 90 degrees, a somewhat larger value of $h_{\lambda'}$ would be more appropriate. It was therefore decided that the grid should be split in half and the function be evaluated at each point in the upper half of the grid. Then, the lower half of the grid was to be halved again and the function evaluated at each point in the upper half of this portion of the grid. This subdivision process was to be continued until convergence to within one per cent was achieved. After a few tests for convergence, it was found that this subdivision process along the λ' variable had to be repeated ten times.

The computer program

A computer program was compiled for the purpose of solving Equations 52 and 53 by means of the iterated Simpson's rule, Equation 58. The program was written in such a way that solutions for N_1 and E_1 could be calculated for a variety of cases. This investigation was concerned with four different scattering media; namely, water, iron, lead and uranium. For each of these media, N_1 and E_1 were

calculated for a variety of spherical radii, ranging from 1 to 20 mean free paths, and a variety of incident photon energies ranging from 1 to 8 $m_o c^2$.

Coupled to the main program is a Lagrange's interpolation subroutine. Wiley (18) presents a rather extensive discussion on Lagrange's interpolation formula and reference should be made to his work for further detail. The purpose of the subroutine is to calculate the value of the attenuation coefficient μ for the scattered photon. The subroutine is supplied with pairs of data points as shown in Table 6. All data supplied to the subroutine were taken from U.S. Atomic Energy Commission (16).

It is generally more instructive to calculate number density ratios, N_1/N_o and energy density ratios E_1/E_o, where N_o and E_o refer to non-scattered photons. Thus the program was composed so as to generate these ratios as well as N_1 and E_1. The results of these calculations have been tabulated and are presented in Tables 2 through 5.

Table 2. First order scattering attenuation calculations for H_2O

Energy ($m_o c^2$)	Radius (mfp)	N_1	N_o	N_1/N_o ($\times 10^{-3}$)	E_1	E_o	E_1/E_o ($\times 10^{-3}$)
1.0	1.0	$5.64(10^{-3})$	$3.68(10^{-1})$	15.3	$3.48(10^{-3})$	$3.68(10^{-1})$	9.46
	3.0	$1.24(10^{-3})$	$4.98(10^{-2})$	25.0	$8.63(10^{-4})$	$4.98(10^{-2})$	17.3
	5.0	$1.86(10^{-4})$	$6.74(10^{-3})$	27.6	$1.38(10^{-4})$	$6.74(10^{-3})$	20.5
	8.0	$9.44(10^{-6})$	$3.35(10^{-4})$	28.1	$7.51(10^{-6})$	$3.35(10^{-4})$	22.4
	12.0	$1.69(10^{-7})$	$6.14(10^{-6})$	27.5	$1.42(10^{-7})$	$6.14(10^{-6})$	23.1
	16.0	$3.00(10^{-9})$	$1.12(10^{-7})$	26.7	$2.60(10^{-9})$	$1.12(10^{-7})$	23.1
	20.0	$5.33(10^{-11})$	$2.06(10^{-9})$	25.9	$4.72(10^{-1})$	$2.06(10^{-9})$	22.9
2.0	1.0	$3.35(10^{-3})$	$3.68(10^{-1})$	9.12	$3.45(10^{-3})$	$7.36(10^{-1})$	4.69
	3.0	$6.42(10^{-4})$	$4.98(10^{-2})$	12.9	$8.13(10^{-4})$	$9.96(10^{-2})$	8.17
	5.0	$9.17(10^{-5})$	$6.74(10^{-3})$	13.6	$1.29(10^{-4})$	$1.35(10^{-2})$	9.58
	8.0	$4.62(10^{-6})$	$3.35(10^{-4})$	13.8	$7.07(10^{-6})$	$6.71(10^{-4})$	10.5
	12.0	$8.35(10^{-7})$	$6.14(10^{-6})$	13.6	$1.35(10^{-7})$	$1.23(10^{-5})$	11.0
	16.0	$1.50(10^{-9})$	$1.12(10^{-7})$	13.3	$2.51(10^{-9})$	$2.25(10^{-7})$	11.2
	20.0	$2.67(10^{-11})$	$2.06(10^{-9})$	13.0	$4.60(10^{-11})$	$4.12(10^{-9})$	11.2

Table 2 (Continued)

Energy ($m_o c^2$)	Radius (mfp)	N_1	N_0	N_1/N_0 ($\times 10^{-3}$)	E_1	E_0	E_1/E_0 ($\times 10^{-3}$)
4.0	1.0	$1.68(10^{-3})$	$3.68(10^{-1})$	4.57	$2.97(10^{-3})$	1.47	2.02
	3.0	$2.84(10^{-4})$	$4.98(10^{-2})$	5.70	$6.70(10^{-4})$	$1.99(10^{-1})$	3.36
	5.0	$3.92(10^{-5})$	$6.74(10^{-3})$	5.82	$1.04(10^{-4})$	$2.70(10^{-2})$	3.87
	8.0	$1.92(10^{-6})$	$3.35(10^{-4})$	5.71	$5.60(10^{-6})$	$1.34(10^{-3})$	4.17
	12.0	$3.35(10^{-8})$	$6.14(10^{-6})$	5.46	$1.04(10^{-7})$	$2.46(10^{-5})$	4.25
	16.0	$5.84(10^{-10})$	$1.12(10^{-7})$	5.19	$1.89(10^{-9})$	$4.50(10^{-7})$	4.20
	20.0	$1.02(10^{-11})$	$2.06(10^{-9})$	4.95	$3.39(10^{-11})$	$8.24(10^{-9})$	4.11
8.0	1.0	$7.60(10^{-4})$	$3.68(10^{-1})$	2.07	$2.36(10^{-3})$	2.94	.802
	3.0	$1.16(10^{-4})$	$4.98(10^{-2})$	2.34	$5.09(10^{-4})$	$3.98(10^{-1})$	1.28
	5.0	$1.54(10^{-5})$	$6.74(10^{-3})$	2.29	$7.62(10^{-5})$	$5.39(10^{-2})$	1.41
	8.0	$7.06(10^{-7})$	$3.35(10^{-4})$	2.10	$3.80(10^{-6})$	$2.68(10^{-3})$	1.42
	12.0	$1.12(10^{-8})$	$6.14(10^{-6})$	1.82	$6.36(10^{-8})$	$4.92(10^{-5})$	1.29
	16.0	$1.75(10^{-10})$	$1.12(10^{-7})$	1.56	$1.03(10^{-9})$	$9.00(10^{-7})$	1.15
	20.0	$2.76(10^{-12})$	$2.06(10^{-9})$	1.34	$1.68(10^{-11})$	$1.65(10^{-8})$	1.02

Table 3. First order scattering attenuation calculations for Fe

Energy ($m_o c^2$)	Radius (mfp)	N_1	N_0	N_1/N_0 ($\times 10^{-2}$)	E_1	E_0	E_1/E_0 ($\times 10^{-2}$)
1.0	1.0	$3.14(10^{-2})$	$3.68(10^{-1})$	8.53	$1.92(10^{-2})$	$3.68(10^{-1})$	5.23
	3.0	$6.17(10^{-3})$	$4.98(10^{-2})$	12.4	$4.37(10^{-3})$	$4.98(10^{-2})$	8.78
	5.0	$8.93(10^{-4})$	$6.74(10^{-3})$	13.3	$6.83(10^{-4})$	$6.74(10^{-3})$	10.1
	8.0	$4.50(10^{-5})$	$3.35(10^{-4})$	13.4	$3.66(10^{-5})$	$3.35(10^{-4})$	10.9
	12.0	$8.04(10^{-7})$	$6.14(10^{-6})$	13.1	$6.87(10^{-7})$	$6.14(10^{-6})$	11.2
	16.0	$1.42(10^{-8})$	$1.12(10^{-7})$	12.7	$1.25(10^{-8})$	$1.12(10^{-7})$	11.1
	20.0	$2.52(10^{-10})$	$2.06(10^{-9})$	12.2	$2.26(10^{-10})$	$2.06(10^{-9})$	10.9
2.0	1.0	$1.91(10^{-2})$	$3.68(10^{-1})$	5.18	$1.95(10^{-2})$	$7.36(10^{-1})$	2.65
	3.0	$3.40(10^{-3})$	$4.98(10^{-2})$	6.83	$4.36(10^{-3})$	$9.96(10^{-2})$	4.37
	5.0	$4.75(10^{-4})$	$6.74(10^{-3})$	7.04	$6.75(10^{-4})$	$1.35(10^{-2})$	5.01
	8.0	$2.33(10^{-5})$	$3.35(10^{-4})$	6.94	$3.59(10^{-5})$	$6.71(10^{-4})$	5.36
	12.0	$4.08(10^{-7})$	$6.14(10^{-6})$	6.64	$6.68(10^{-7})$	$1.23(10^{-5})$	5.43
	16.0	$7.12(10^{-9})$	$1.12(10^{-7})$	6.32	$1.21(10^{-8})$	$2.25(10^{-7})$	5.36
	20.0	$1.24(10^{-10})$	$2.06(10^{-9})$	6.03	$2.16(10^{-10})$	$4.12(10^{-9})$	5.24

Table 3 (Continued)

Energy ($m_o c^2$)	Radius (mfp)	N_1	N_0	N_1/N_0 ($\times 10^{-2}$)	E_1	E_0	E_1/E_0 ($\times 10^{-2}$)
4.0	1.0	$1.01(10^{-2})$	$3.68(10^{-1})$	2.76	$1.77(10^{-2})$	1.47	1.20
	3.0	$1.69(10^{-3})$	$4.98(10^{-2})$	3.40	$3.98(10^{-3})$	$1.99(10^{-1})$	2.00
	5.0	$2.34(10^{-4})$	$6.74(10^{-3})$	3.48	$6.25(10^{-4})$	$2.70(10^{-2})$	2.32
	8.0	$1.16(10^{-5})$	$3.35(10^{-4})$	3.44	$3.39(10^{-5})$	$1.34(10^{-3})$	2.53
	12.0	$2.05(10^{-7})$	$6.14(10^{-6})$	3.33	$6.43(10^{-7})$	$2.46(10^{-5})$	2.61
	16.0	$3.61(10^{-9})$	$1.12(10^{-7})$	3.21	$1.18(10^{-8})$	$4.50(10^{-7})$	2.62
	20.0	$6.37(10^{-11})$	$2.06(10^{-9})$	3.09	$2.14(10^{-10})$	$8.24(10^{-9})$	2.60
8.0	1.0	$5.48(10^{-3})$	$3.68(10^{-1})$	1.49	$1.59(10^{-2})$	2.94	.539
	3.0	$9.30(10^{-4})$	$4.98(10^{-2})$	1.87	$3.84(10^{-3})$	$3.98(10^{-1})$	.965
	5.0	$1.33(10^{-4})$	$6.74(10^{-3})$	1.97	$6.29(10^{-4})$	$5.39(10^{-2})$	1.17
	8.0	$6.68(10^{-6})$	$3.35(10^{-4})$	1.99	$3.51(10^{-5})$	$2.68(10^{-3})$	1.31
	12.0	$1.18(10^{-7})$	$6.14(10^{-6})$	1.92	$6.67(10^{-7})$	$4.92(10^{-5})$	1.36
	16.0	$2.04(10-9)$	$1.12(10^{-7})$	1.81	$1.20(10^{-8})$	$9.00(10^{-7})$	1.33
	20.0	$3.47(10^{-11})$	$2.06(10^{-9})$	1.68	$2.11(10^{-10})$	$1.65(10^{-8})$	1.28

Table 4. First order scattering attenuation calculations for Pb

Energy ($m_o c^2$)	Radius (mfp)	N_1	N_o	N_1/N_o ($\times 10^{-2}$)	E_1	E_o	E_1/E_o ($\times 10^{-2}$)
1.0	1.0	$1.40(10^{-2})$	$3.68(10^{-1})$	3.81	$1.01(10^{-2})$	$3.68(10^{-1})$	2.76
	3.0	$2.18(10^{-3})$	$4.98(10^{-2})$	4.38	$1.82(10^{-3})$	$4.98(10^{-2})$	3.66
	5.0	$3.04(10^{-4})$	$6.74(10^{-3})$	4.52	$2.66(10^{-4})$	$6.74(10^{-3})$	3.95
	8.0	$1.52(10^{-5})$	$3.35(10^{-4})$	4.54	$1.38(10^{-5})$	$3.35(10^{-4})$	4.10
	12.0	$2.74(10^{-7})$	$6.14(10^{-6})$	4.47	$2.54(10^{-7})$	$6.14(10^{-6})$	4.13
	16.0	$4.93(10^{-9})$	$1.12(10^{-7})$	4.38	$4.63(10^{-9})$	$1.12(10^{-7})$	4.12
	20.0	$8.90(10^{-11})$	$2.06(10^{-9})$	4.32	$8.44(10^{-11})$	$2.06(10^{-9})$	4.09
2.0	1.0	$1.05(10^{-2})$	$3.68(10^{-1})$	2.85	$1.36(10^{-2})$	$7.36(10^{-1})$	1.84
	3.0	$1.88(10^{-3})$	$4.98(10^{-2})$	3.78	$2.84(10^{-3})$	$9.96(10^{-2})$	2.85
	5.0	$2.67(10^{-4})$	$6.74(10^{-3})$	3.97	$4.30(10^{-4})$	$1.35(10^{-2})$	3.19
	8.0	$1.32(10^{-5})$	$3.35(10^{-4})$	3.94	$2.23(10^{-5})$	$6.71(10^{-4})$	3.33
	12.0	$2.32(10^{-7})$	$6.14(10^{-6})$	3.77	$4.06(10^{-7})$	$1.23(10^{-5})$	3.31
	16.0	$4.04(10^{-9})$	$1.12(10^{-7})$	3.59	$7.23(10^{-9})$	$2.25(10^{-7})$	3.21
	20.0	$7.04(10^{-11})$	$2.06(10^{-9})$	3.41	$1.28(10^{-10})$	$4.12(10^{-9})$	3.11

Table 4 (Continued)

Energy ($m_o c^2$)	Radius (mfp)	N_1	N_0	N_1/N_0 ($\times 10^{-2}$)	E_1	E_0	E_1/E_0 ($\times 10^{-2}$)
4.0	1.0	$7.74(10^{-3})$	$3.68(10^{-1})$	2.10	$1.64(10^{-2})$	1.47	1.12
	3.0	$1.53(10^{-3})$	$4.98(10^{-2})$	3.08	$4.01(10^{-3})$	$1.99(10^{-1})$	2.01
	5.0	$2.34(10^{-4})$	$6.74(10^{-3})$	3.48	$6.65(10^{-4})$	$2.70(10^{-2})$	2.47
	8.0	$1.26(10^{-5})$	$3.35(10^{-4})$	3.74	$3.80(10^{-5})$	$1.34(10^{-3})$	2.83
	12.0	$2.35(10^{-7})$	$6.14(10^{-6})$	3.83	$7.47(10^{-7})$	$2.46(10^{-5})$	3.04
	16.0	$4.26(10^{-9})$	$1.12(10^{-7})$	3.79	$1.40(10^{-8})$	$4.50(10^{-7})$	3.10
	20.0	$7.61(10^{-11})$	$2.06(10^{-9})$	3.69	$2.55(10^{-10})$	$8.24(10^{-9})$	3.09
8.0	1.0	$5.79(10^{-3})$	$3.68(10^{-1})$	1.57	$1.84(10^{-2})$	2.94	.624
	3.0	$1.37(10^{-3})$	$4.98(10^{-2})$	2.74	$5.46(10^{-3})$	$3.98(10^{-1})$	1.37
	5.0	$2.39(10^{-4})$	$6.74(10^{-3})$	3.55	$1.04(10^{-3})$	$5.39(10^{-2})$	1.93
	8.0	$1.54(10^{-5})$	$3.35(10^{-4})$	4.60	$7.17(10^{-5})$	$2.68(10^{-3})$	2.67
	12.0	$3.70(10^{-7})$	$6.14(10^{-6})$	6.02	$1.80(10^{-6})$	$4.92(10^{-5})$	3.66
	16.0	$8.64(10^{-9})$	$1.12(10^{-7})$	7.68	$4.30(10^{-8})$	$9.00(10^{-7})$	4.77
	20.0	$2.00(10^{-10})$	$2.06(10^{-9})$	9.69	$1.01(10^{-9})$	$1.65(10^{-8})$	6.11

Table 5. First order scattering attenuation calculations for U

Energy ($m_o c^2$)	Radius (mfp)	N_1	N_0	N_1/N_0 ($\times 10^{-2}$)	E_1	E_0	E_1/E_0 ($\times 10^{-2}$)
4.0	1.0	$1.06(10^{-2})$	$3.68(10^{-1})$	2.89	$2.32(10^{-2})$	1.47	1.58
	3.0	$2.07(10^{-3})$	$4.98(10^{-2})$	4.16	$5.55(10^{-3})$	$1.99(10^{-1})$	2.78
	5.0	$3.15(10^{-4})$	$6.74(10^{-3})$	4.67	$9.10(10^{-4})$	$2.79(10^{-2})$	3.38
	8.0	$1.67(10^{-5})$	$3.35(10^{-4})$	4.97	$5.12(10^{-5})$	$1.34(10^{-3})$	3.82
	12.0	$3.08(10^{-7})$	$6.14(10^{-6})$	5.01	$9.89(10^{-7})$	$2.46(10^{-5})$	4.02
	16.0	$5.49(10^{-9})$	$1.12(10^{-7})$	4.88	$1.82(10^{-8})$	$4.50(10^{-7})$	4.04
	20.0	$9.66(10^{-11})$	$2.06(10^{-9})$	4.68	$3.27(10^{-10})$	$8.24(10^{-9})$	3.97
4.5	1.0	$1.03(10^{-2})$	$3.68(10^{-1})$	2.81	$2.44(10^{-2})$	1.66	1.47
	3.0	$2.13(10^{-3})$	$4.98(10^{-2})$	4.28	$6.22(10^{-3})$	$2.24(10^{-1})$	2.77
	5.0	$3.40(10^{-4})$	$6.74(10^{-3})$	5.05	$1.08(10^{-3})$	$3.03(10^{-2})$	3.56
	8.0	$1.94(10^{-5})$	$3.35(10^{-4})$	5.80	$6.64(10^{-5})$	$1.51(10^{-3})$	4.40
	12.0	$4.05(10^{-7})$	$6.14(10^{-6})$	6.59	$1.47(10^{-6})$	$2.76(10^{-5})$	5.31
	16.0	$8.39(10^{-9})$	$1.12(10^{-7})$	7.46	$3.18(10^{-8})$	$5.06(10^{-7})$	6.27
	20.0	$1.76(10^{-10})$	$2.06(10^{-9})$	8.56	$6.90(10^{-10})$	$9.28(10^{-9})$	7.44

Table 5 (Continued)

Energy ($m_o c^2$)	Radius (mfp)	N_1	N_0	N_1/N_0 ($\times 10^{-2}$)	E_1	E_0	E_1/E_0 ($\times 10^{-2}$)
5.0	1.0	$1.00(10^{-2})$	$3.68(10^{-1})$	2.73	$2.53(10^{-2})$	1.84	1.38
	3.0	$2.18(10^{-3})$	$4.98(10^{-2})$	4.38	$6.91(10^{-3})$	$2.49(10^{-1})$	2.78
	5.0	$3.69(10^{-4})$	$6.74(10^{-3})$	5.48	$1.29(10^{-3})$	$3.37(10^{-2})$	3.81
	8.0	$2.35(10^{-5})$	$3.35(10^{-4})$	7.00	$8.92(10^{-5})$	$1.68(10^{-3})$	5.32
	12.0	$5.87(10^{-7})$	$6.14(10^{-6})$	9.55	$2.40(10^{-6})$	$3.07(10^{-5})$	7.82
	16.0	$1.52(10^{-8})$	$1.12(10^{-7})$	1.35	$6.53(10^{-8})$	$5.63(10^{-7})$	11.6
	20.0	$4.08(10^{-10})$	$2.06(10^{-9})$	1.98	$1.81(10^{-9})$	$1.03(10^{-8})$	17.6
5.5	1.0	$9.69(10^{-3})$	$3.68(10^{-1})$	2.63	$2.60(10^{-2})$	2.02	1.29
	3.0	$2.20(10^{-3})$	$4.98(10^{-2})$	4.41	$7.49(10^{-3})$	$2.74(10^{-1})$	2.74
	5.0	$3.89(10^{-4})$	$6.74(10^{-3})$	5.77	$1.47(10^{-3})$	$3.71(10^{-2})$	3.97
	8.0	$2.68(10^{-5})$	$3.35(10^{-4})$	7.99	$1.11(10^{-4})$	$1.84(10^{-3})$	6.04
	12.0	$7.54(10^{-7})$	$6.14(10^{-6})$	1.23	$3.37(10^{-6})$	$3.38(10^{-5})$	9.98
	16.0	$2.18(10^{-8})$	$1.12(10^{-7})$	1.94	$1.02(10^{-7})$	$6.19(10^{-7})$	1.65
	20.0	$6.46(10^{-10})$	$2.06(10^{-9})$	3.13	$3.10(10^{-9})$	$1.13(10^{-8})$	2.73

Table 5 (Continued)

Energy ($m_o c^2$)	Radius (mfp)	N_1	N_0	N_1/N_0 ($\times 10^{-2}$)	E_1	E_0	E_1/E_0 ($\times 10^{-2}$)
6.0	1.0	$9.29(10^{-3})$	$3.68(10^{-1})$	2.52	$2.64(10^{-2})$	2.21	1.19
	3.0	$2.14(10^{-3})$	$4.98(10^{-2})$	4.30	$7.76(10^{-3})$	$2.99(10^{-1})$	2.60
	5.0	$3.84(10^{-4})$	$6.74(10^{-3})$	5.70	$1.54(10^{-3})$	$4.04(10^{-2})$	3.82
	8.0	$2.68(10^{-5})$	$3.35(10^{-4})$	7.99	$1.18(10^{-4})$	$2.01(10^{-3})$	5.85
	12.0	$7.49(10^{-7})$	$6.14(10^{-6})$	12.2	$3.51(10^{-6})$	$3.69(10^{-5})$	9.53
	16.0	$2.11(10^{-8})$	$1.12(10^{-7})$	18.7	$1.02(10^{-7})$	$6.75(10^{-7})$	15.1
	20.0	$5.94(10^{-10})$	$2.06(10^{-9})$	28.8	$2.94(10^{-9})$	$1.24(10^{-8})$	23.8
8.0	1.0	$8.15(10^{-3})$	$3.68(10^{-1})$	2.22	$2.65(10^{-2})$	2.94	.901
	3.0	$1.92(10^{-3})$	$4.98(10^{-2})$	3.86	$7.80(10^{-3})$	$3.98(10^{-1})$	1.96
	5.0	$3.42(10^{-4})$	$6.74(10^{-3})$	5.08	$1.51(10^{-3})$	$5.39(10^{-2})$	2.80
	8.0	$2.31(10^{-5})$	$3.35(10^{-4})$	6.89	$1.08(10^{-4})$	$2.68(10^{-3})$	4.03
	12.0	$6.04(10^{-7})$	$6.14(10^{-6})$	9.82	$2.94(10^{-6})$	$4.92(10^{-5})$	5.98
	16.0	$1.55(10^{-8})$	$1.12(10^{-7})$	13.8	$7.74(10^{-8})$	$9.00(10^{-7})$	8.59
	20.0	$3.99(10^{-10})$	$2.06(10^{-9})$	19.4	$2.01(10^{-9})$	$1.65(10^{-8})$	12.2

DISCUSSION OF RESULTS

For the purpose of data investigation, the attenuation calculations generated by the program were plotted and are illustrated in Figures 8 through 15.

Consider the lighter materials first; namely, water and iron. The number density ratios, N_1/N_o, are seen to decrease with increasing source energy in both cases. Also, it can be seen that the curves reach a maximum value in the range of 3 to 8 mean free paths. For larger values of R, the value of N_1/N_o is seen to decrease as R increases, the rate of decrease being larger in the case of the lower source energy.

Similar conclusions may be reached concerning E_1/E_o for water and iron; the only discrepancy being that the curves of E_1/E_o are somewhat smoother. That is, E_1/E_o reaches its maximum value at larger values of R than did N_1/N_o, and its rate of decrease is somewhat smaller than in the case of N_1/N_o.

The above conclusions may be aptly applied to the heavier materials lead and uranium only for the lower source energy cases. In the case of higher source energies, the curves are seen to change shape drastically with increasing source energy. For the largest value of the source energy, namely $8\ m_o c^2$, N_1/N_o and E_1/E_o are seen to increase continuously with increasing values of the parameter R. This behavior for larger values of source energies in the case

Figure 8. Number density ratio of water as a function of sphere radius for 1, 2, 4, and 8 $m_o c^2$ incident photons.

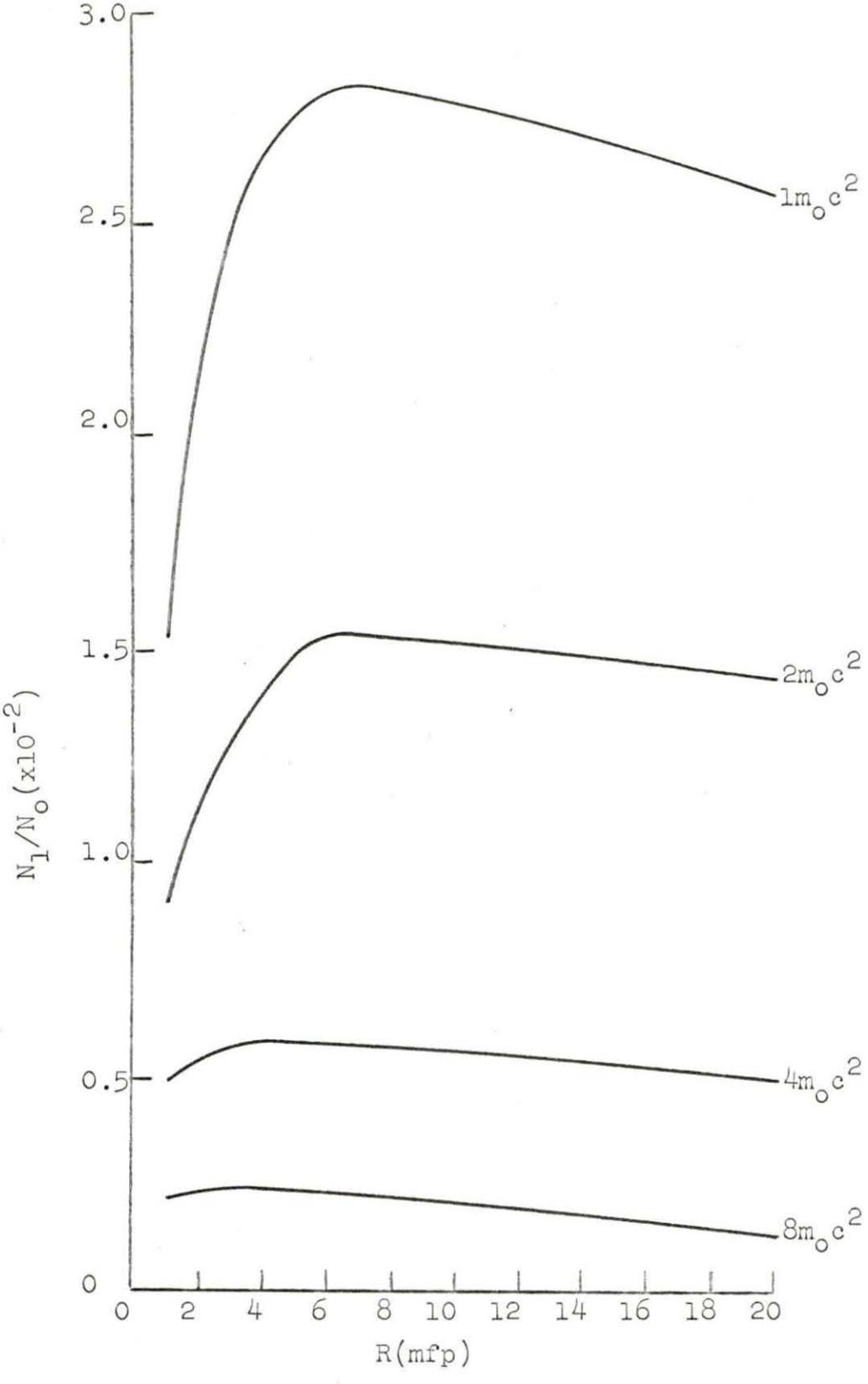
3.0
2.5
2.0
1.5
1.0
0.5
0
$N_1/N_o(x10^{-2})$
$1m_oc^2$
$2m_oc^2$
$4m_oc^2$
$8m_oc^2$
0 2 4 6 8 10 12 14 16 18 20
R(mfp)

Figure 9. Energy density ratio of water as a function of sphere radius for 1, 2, 4 and 8 $m_o c^2$ incident photons.

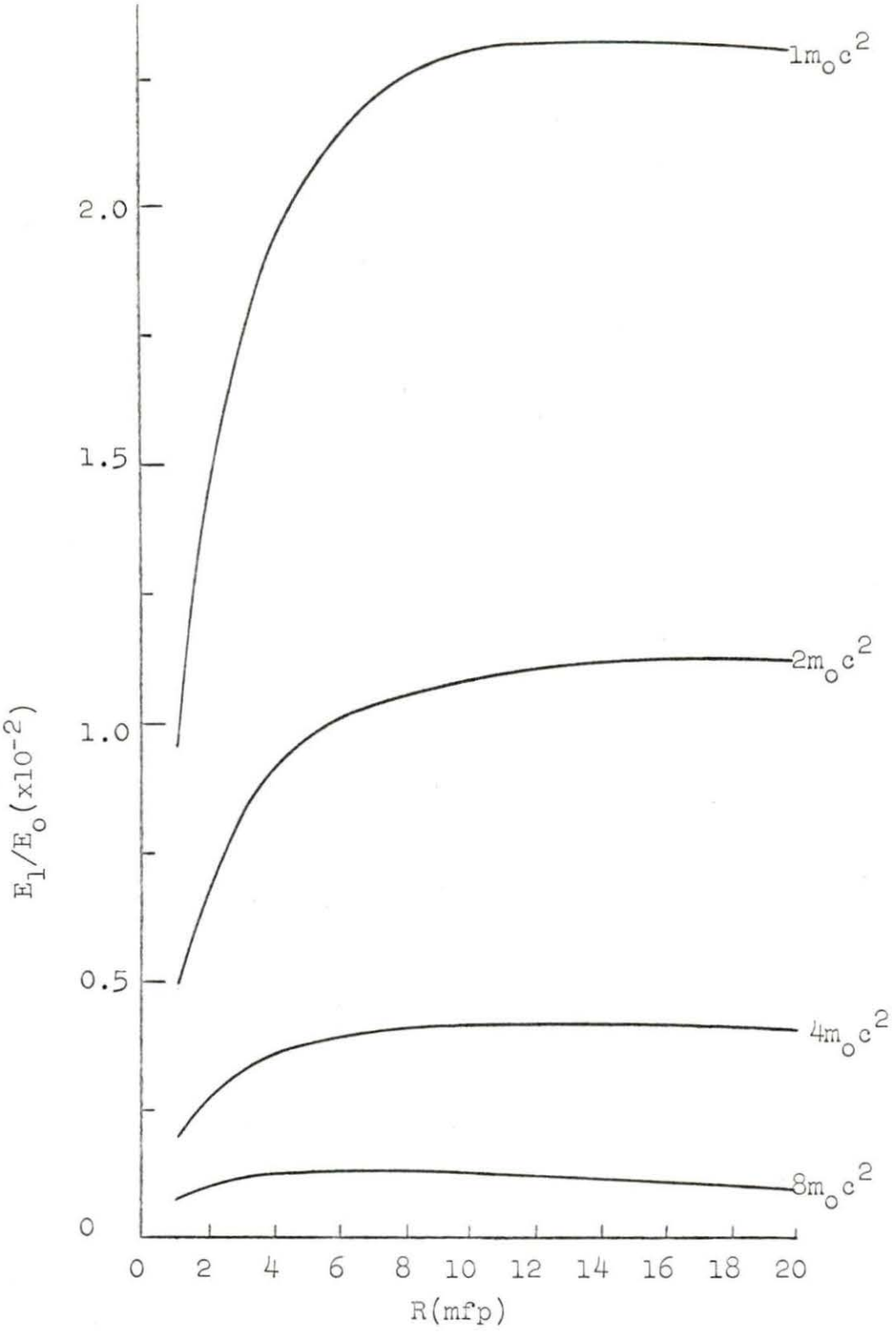
$1m_oc^2$
$2m_oc^2$
$4m_oc^2$
$8m_oc^2$
2.0
1.5
1.0
0.5
0
$E_1/E_o(x10^{-2})$
0 2 4 6 8 10 12 14 16 18 20
R(mfp)

Figure 10. Number density ratio of iron as a function of sphere radius for 1, 2, 4 and 8 $m_o c^2$ incident photons.

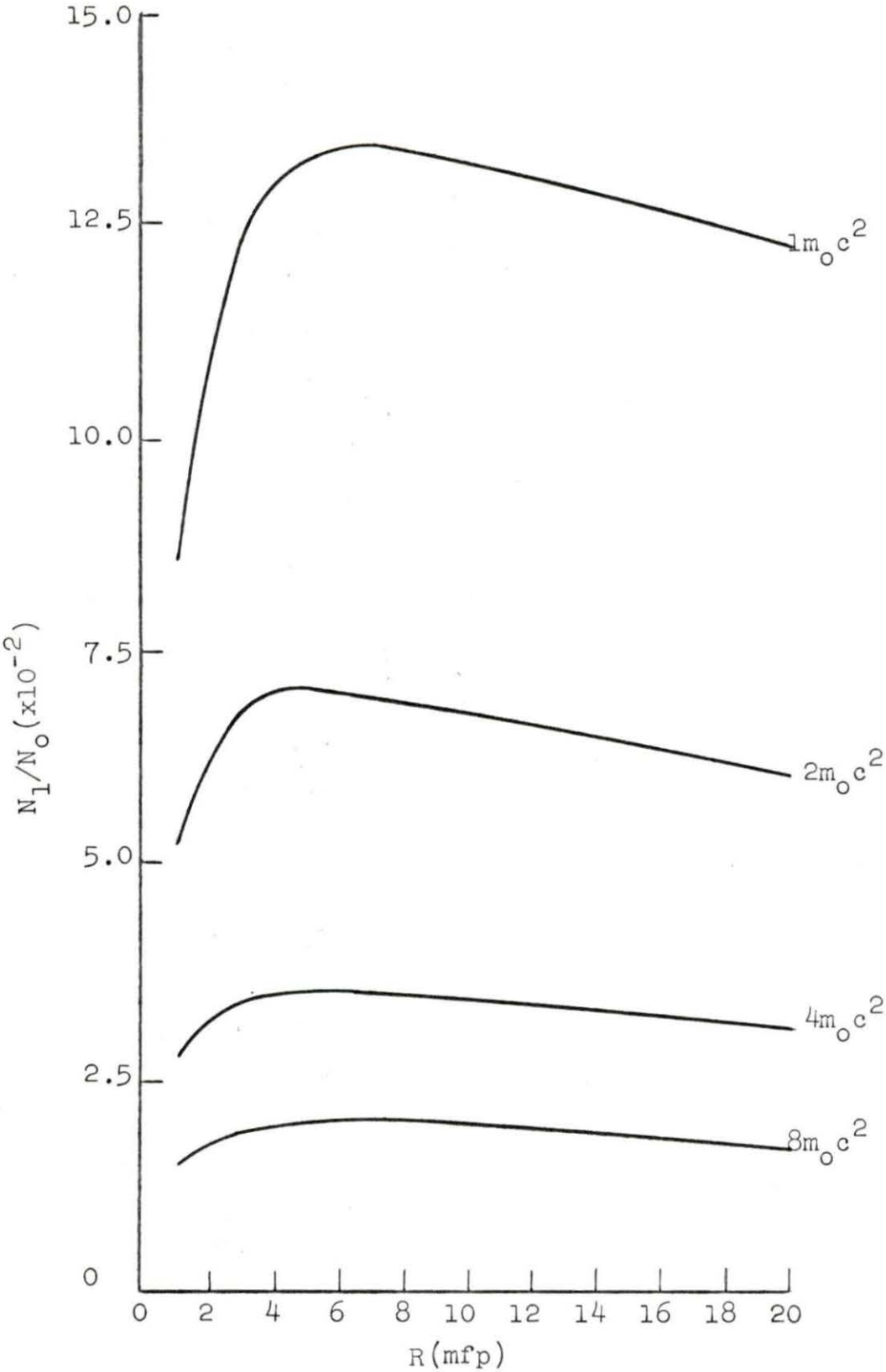
15.0
12.5
10.0
7.5
5.0
2.5
0
$N_1/N_o(x10^{-2})$
$1m_oc^2$
$2m_oc^2$
$4m_oc^2$
$8m_oc^2$
0 2 4 6 8 10 12 14 16 18 20
R(mfp)

Figure 11. Energy density ratio of iron as a function of sphere radius for 1, 2, 4 and 8 $m_o c^2$ incident photons.

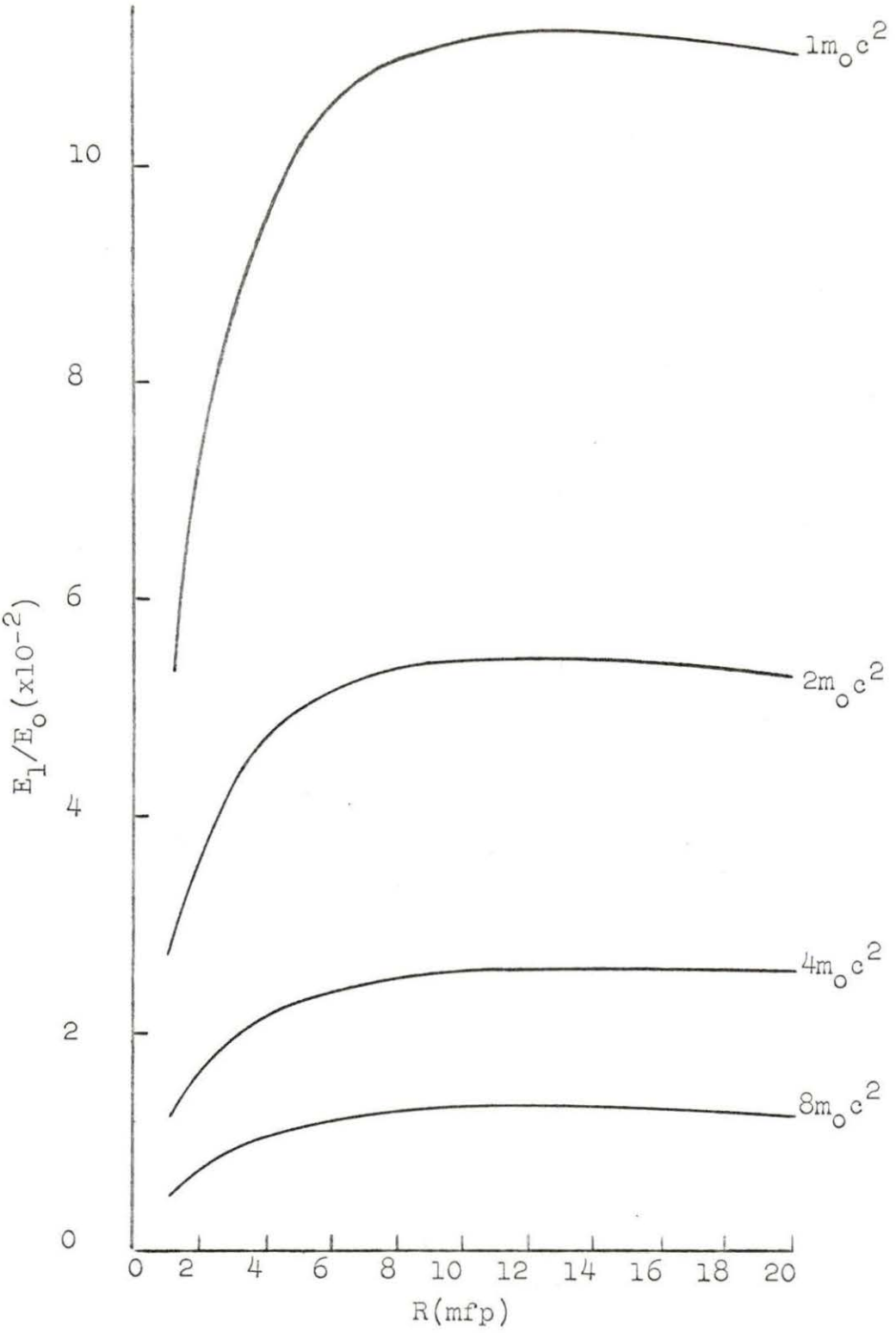
E_1/E_o ($x10^{-2}$)
0
2
4
6
8
10
0 2 4 6 8 10 12 14 16 18 20
R(mfp)
$1m_oc^2$
$2m_oc^2$
$4m_oc^2$
$8m_oc^2$

Figure 12. Number density ratio of lead as a function of sphere radius for 1, 2, 4 and 8 $m_o c^2$ incident photons.

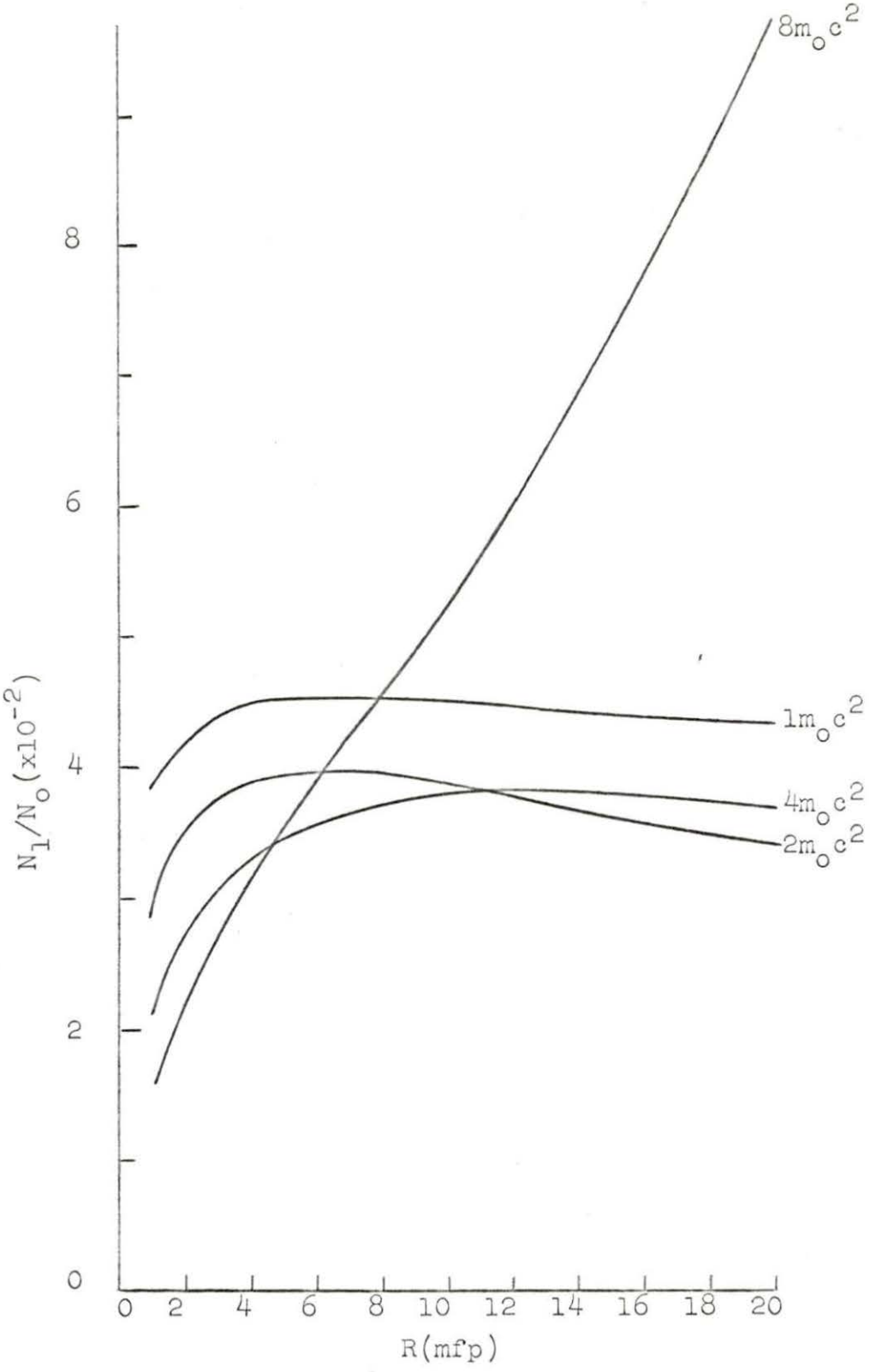
$8m_oc^2$
$1m_oc^2$
$4m_oc^2$
$2m_oc^2$
$N_1/N_o (x10^{-2})$
0
2
4
6
8
0 2 4 6 8 10 12 14 16 18 20
R(mfp)

Figure 13. Energy density ratio of lead as a function of sphere radius for 1, 2, 4 and 8 $m_o c^2$ incident photons.

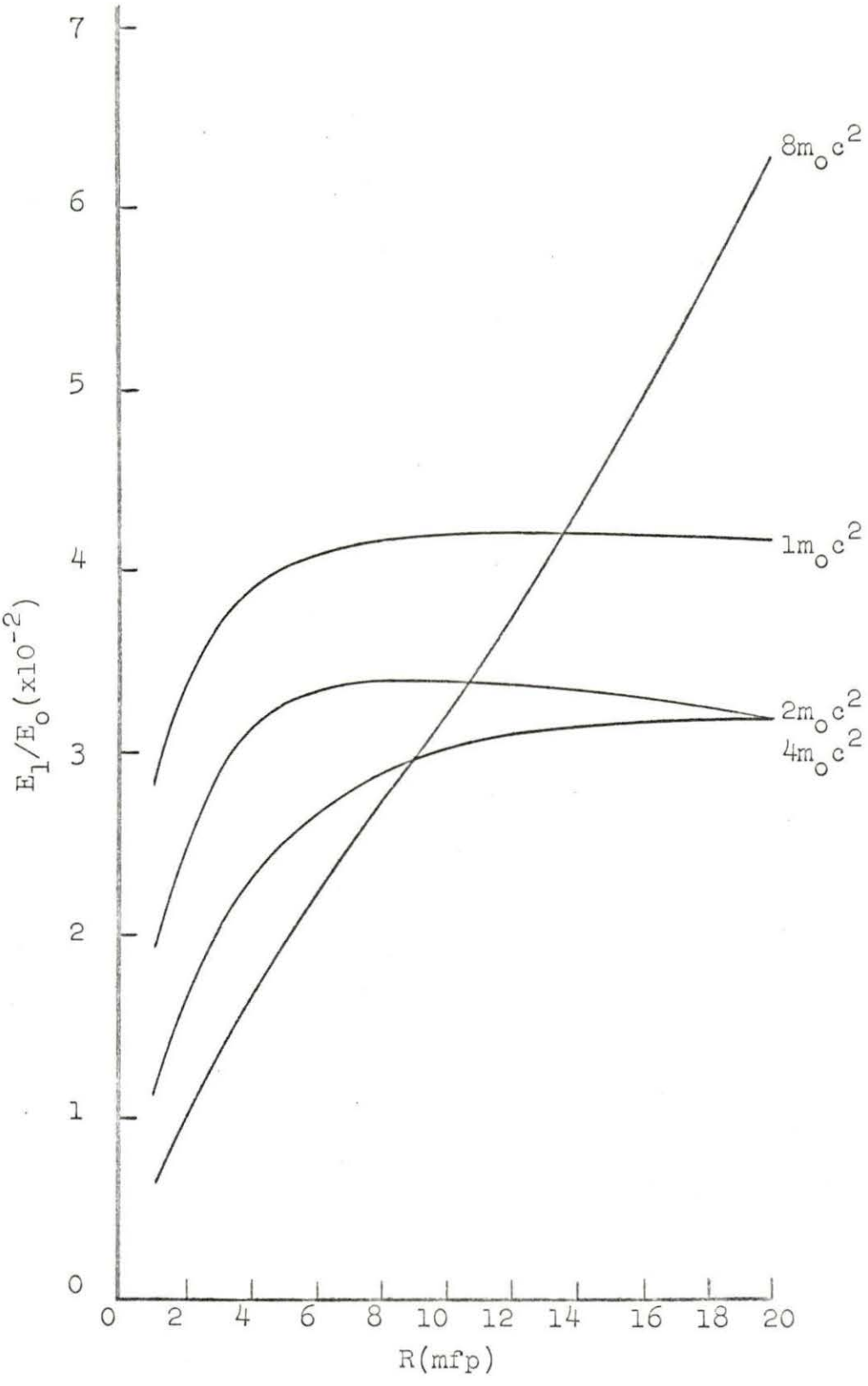
7
6
5
4
3
2
1
0
E_1/E_o (x10^{-2})
$8m_oc^2$
$1m_oc^2$
$2m_oc^2$
$4m_oc^2$
0 2 4 6 8 10 12 14 16 18 20
R(mfp)

Figure 14. Number density ratio of uranium as a function of sphere radius for 4, 4.5, 5, 5.5, 6 and 8 $m_o c^2$ incident photons.

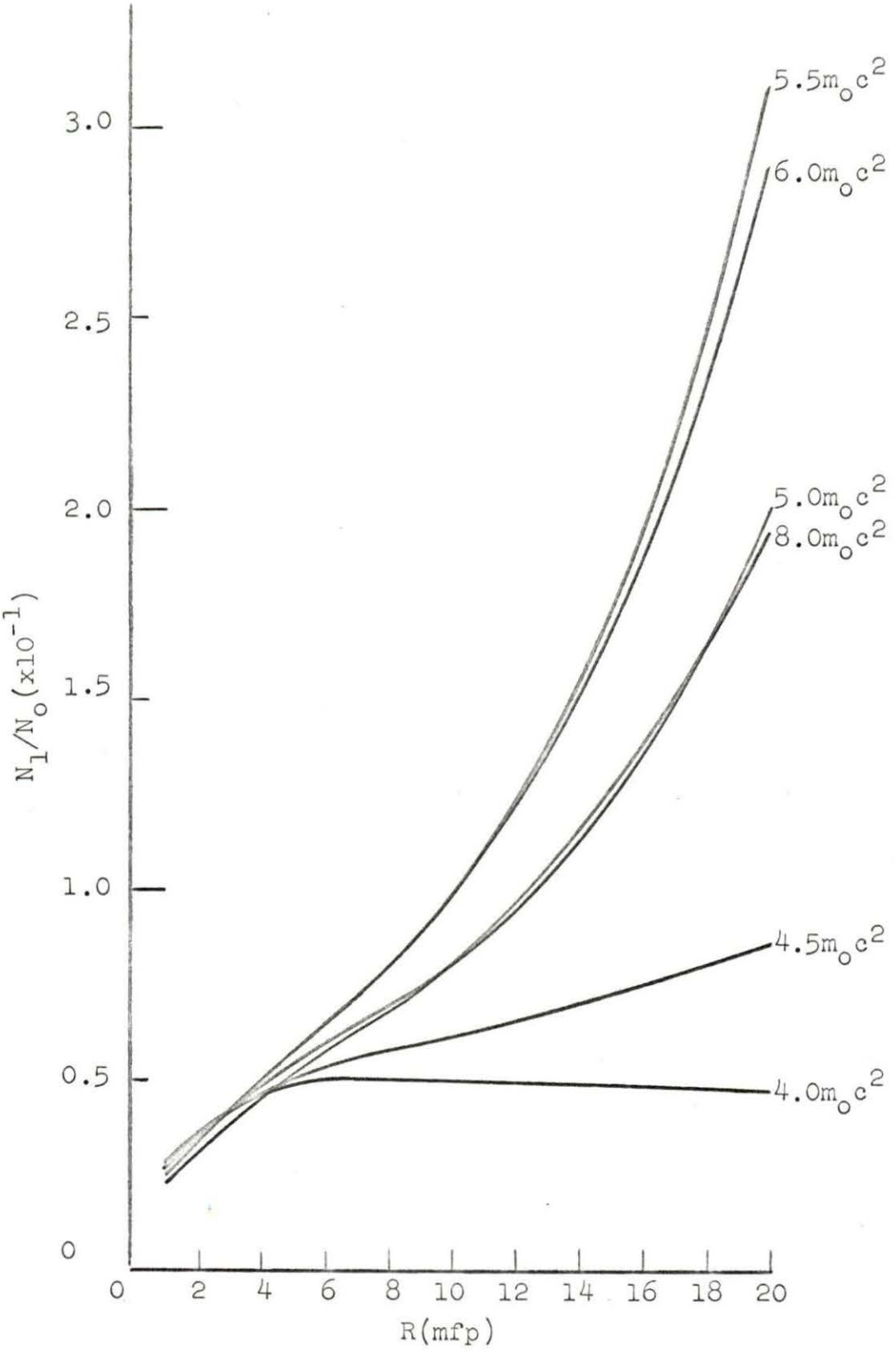
$5.5m_oc^2$
$6.0m_oc^2$
$5.0m_oc^2$
$8.0m_oc^2$
$4.5m_oc^2$
$4.0m_oc^2$
3.0
2.5
2.0
1.5
1.0
0.5
0
$N_1/N_o (x10^{-1})$
0 2 4 6 8 10 12 14 16 18 20
R(mfp)

Figure 15. Energy density ratio of uranium as a function of sphere radius for 4, 4.5, 5, 5.5, 6 and 8 $m_o c^2$ incident photons.

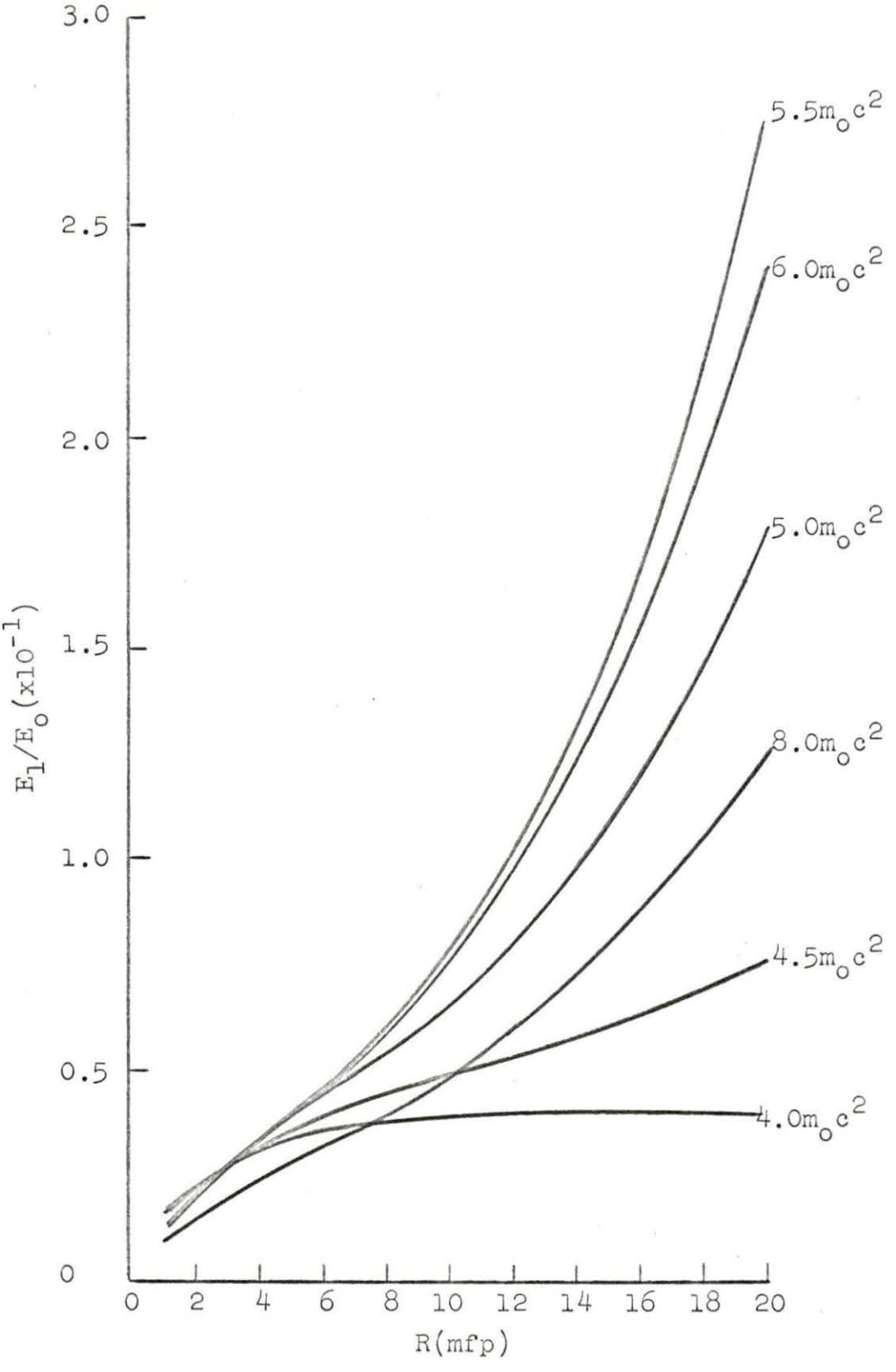
3.0
2.5
2.0
1.5
1.0
0.5
0
E_1/E_o (x10^{-1})
0
2
4
6
8
10
12
14
16
18
20
R(mfp)
5.5m_oc^2
6.0m_oc^2
5.0m_oc^2
8.0m_oc^2
4.5m_oc^2
4.0m_oc^2

of the heavier material may be explained quite readily by examining the curves illustrated in Figure 16. The data for these curves have been taken from U.S. Atomic Energy Commission (16), and are presented in Table 6.

As is obvious from an investigation of the total linear absorption coefficient curves, the value of μ reaches a minimum in the cases of lead and uranium, but not in the cases of water and iron, within the source energy range under investigation. This is the general behavior of the total linear absorption coefficient as a function of energy; i.e., μ reaches a minimum value and then increases with increasing energy. Had the energy range been extended somewhat, μ for iron and water would have also reached a minimum, and similar curves for N_1/N_o and E_1/E_o would have been produced for these materials. The conclusion to be drawn from Figure 16 is that in the cases of lead and uranium, μ is seen to be almost constant over the energy range from 2 to 5 Mev, corresponding to the range from 4 to 10 $m_o c^2$. This constant behavior of μ, not found in the cases of water and iron, is responsible for the behavior of N_1/N_o and E_1/E_o in the cases of lead and uranium in the energy range from 4 to 8 $m_o c^2$.

Values of N_1/N_o and E_1/E_o for uranium have been calculated for intermediate source energies between 4 and 8 $m_o c^2$. An investigation of Figures 14 and 15 indicates that N_1/N_o and E_1/E_o reach maximum values in the vicinity of 5.5 $m_o c^2$

for large values of R. As the source energy is further increased, however, these values are seen to decrease.

Finally, it should be mentioned that in all cases, the value of E_1/E_o is found to be less than that for N_1/N_o. This is to be expected since the energy of the scattered photon must be less than that of the incident photon, from Equation 5. Thus, since E' is less than E, and $E_1 = E'N_1$ and $E_o = EN_o$,

$$E_1/E_o = E'N_1/EN_o < N_1/N_o \ . \qquad (59)$$

Table 6. Total linear absorption coefficients in cm^2 for photon energies in the range of 100 kev to 5 Mev for H_2O, Fe, Pb and U

Energy (Mev)	H_2O	(cm^{-1}) Fe	Pb	U
5.0	0.0301	0.2460	0.4831	0.8340
4.0	0.0339	0.2594	0.4763	0.8228
3.0	0.0396	0.2837	0.4774	0.8322
2.0	0.0493	0.333	0.5182	0.9051
1.5	0.0575	0.3812	0.5806	1.025
1.0	0.0706	0.4677	0.7757	1.416
0.8	0.0786	0.5219	0.9480	1.780
0.6	0.0896	0.5989	1.293	2.543
0.5	0.0966	0.6508	1.644	3.291
0.4	0.106	0.7223	2.359	4.843
0.3	0.118	0.833	4.037	8.452
0.2	0.136	1.085	10.16	21.88
0.15	0.149	1.438	20.87	45.25

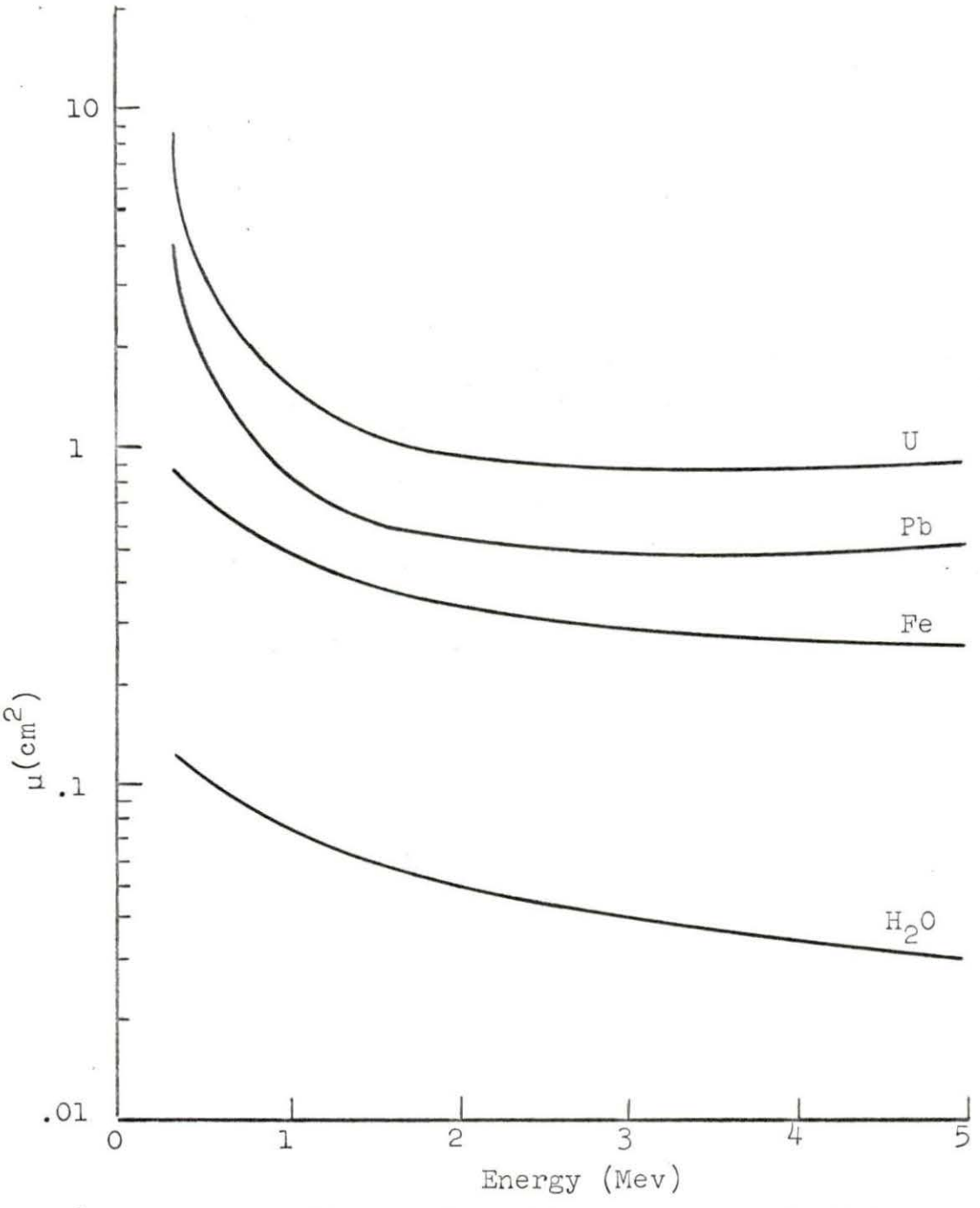

Figure 16. The total linear absorption coefficient as a function of photon energy.

FURTHER APPLICATIONS

This investigation has only considered the number density ratios and the energy density ratios of first order scattering to zero order scattering for a variety of scattering media, incident photon energies and sphere radii. The possibilities of further research on this problem is unlimited. Higher order scattering calculation would yield a very good approximation to number build-up factors and energy build-up factors for a variety of materials in finite geometry. Also, this technique of calculating the attenuation of photons by matter could be applied to layer type problems, where the scattering medium is a succession of concentric spherical layers of different materials.

Finally, the method of successive scattering may be aptly applied to the attenuation of neutrons in matter. Although this would involve very complex functions because of the characteristic nature of the scattering cross section of the neutron, research in this area would be invaluable.

LITERATURE CITED

1. Bethe, H. A. and Ashkin, J. Penetration of gamma rays. In Segre, E., ed. Experimental nuclear physics. Vol. 1. pp. 305-349. New York, N.Y., John Wiley and Sons, Inc. 1953.

2. Davisson, C. M. and Evans, R. D. Gamma ray absorption coefficients. Review of Modern Physics 24: 79-107. 1952.

3a. Fano, U. Gamma ray attenuation. I. Nucleonics 11, No. 8: 8-12. 1953.

3b. Fano, U. Gamma ray attenuation. II. Nucleonics 11, No. 9: 55-16. 1953.

4. Fano, U., Spencer, L. V. and Berger, M. J. Penetration and diffusion of X-rays. Encyclopedia of physics. Vol. 38. Part 2. pp. 660-814. Berlin, Germany, Springer-Verlag. 1959.

5. Friedlander, G. and Kennedy, J. W. Nuclear and radiochemistry. New York, N.Y., John Wiley and Sons, Inc. 1955.

6. Goldstein, H. The attenuation of gamma rays and neutrons in reactor shields. Washington, D.C., U.S. Govt. Print. Off. 1957.

7. Goldstein, H. and Wilkins, J. E., Jr. Calculations of the penetrations of gamma rays. U.S. Atomic Energy Commission Report NYO-3075 [New York Operations Office, AEC] 1954.

8. Heitler, W. Quantum theory of radiation. 3rd ed. New York, N.Y., Oxford University Press. 1954.

9. Kaplan, I. Nuclear physics. Cambridge, Mass., Addison-Wesley Publishing Company, Inc. 1955.

10. Latter, R. and Kahn, H. Gamma ray absorption coefficients. Rand Report R-170. Santa Monica, California, The Rand Corporation. 1949.

11. Leipunskii, O. I., Novozhilov, B. V. and Sakharov, V. N. The propagation of gamma quanta in matter. New York, N.Y., Pergamon Press, Inc. 1965.

12. Nelms, A. T. Graphs of the Compton energy angle relationship and the Klein Nishina formula from 10 kev to 500 Mev. National Bureau of Standards Circular 542. 1953.

13. Peebles, G. H. Gamma-ray transmission through finite slabs. The Rand Corporation (Santa Monica, Calif.), Rand Report R-240. 1952.

14. Segre, E. Experimental nuclear physics. Vol. 1. New York, N.Y., John Wiley and Sons, Inc. 1953.

15. Snyder, W. S. and Powell, J. L. Absorption of gamma rays. U.S. Atomic Energy Commission Report ORNL-421 [Oak Ridge National Lab., Tenn.] 1950.

16. U.S. Atomic Energy Commission. Reactor physics constants. U.S. Atomic Energy Commission Report ANL-5800 [Argonne National Lab., Lemont, Ill.] 1063.

17. White, G. R. Gamma ray attenuation coefficients from 10 kev to 100 Mev. National Bureau of Standards Circular 583. 1957.

18. Wylie, C. R., Jr. Advanced engineering mathematics. New York, N.Y., McGraw-Hill Book Company, Inc. 1960.

ACKNOWLEDGEMENTS

Sincere appreciation is extended to Dr. Alfred F. Rohach for his suggestion of this investigation and his invaluable assistance with numerical integration and programming.

APPENDIX: FLOW DIAGRAMS OF THE MAIN PROGRAM AND THE SUBROUTINE

Figure 17. Flow diagram of the main program.

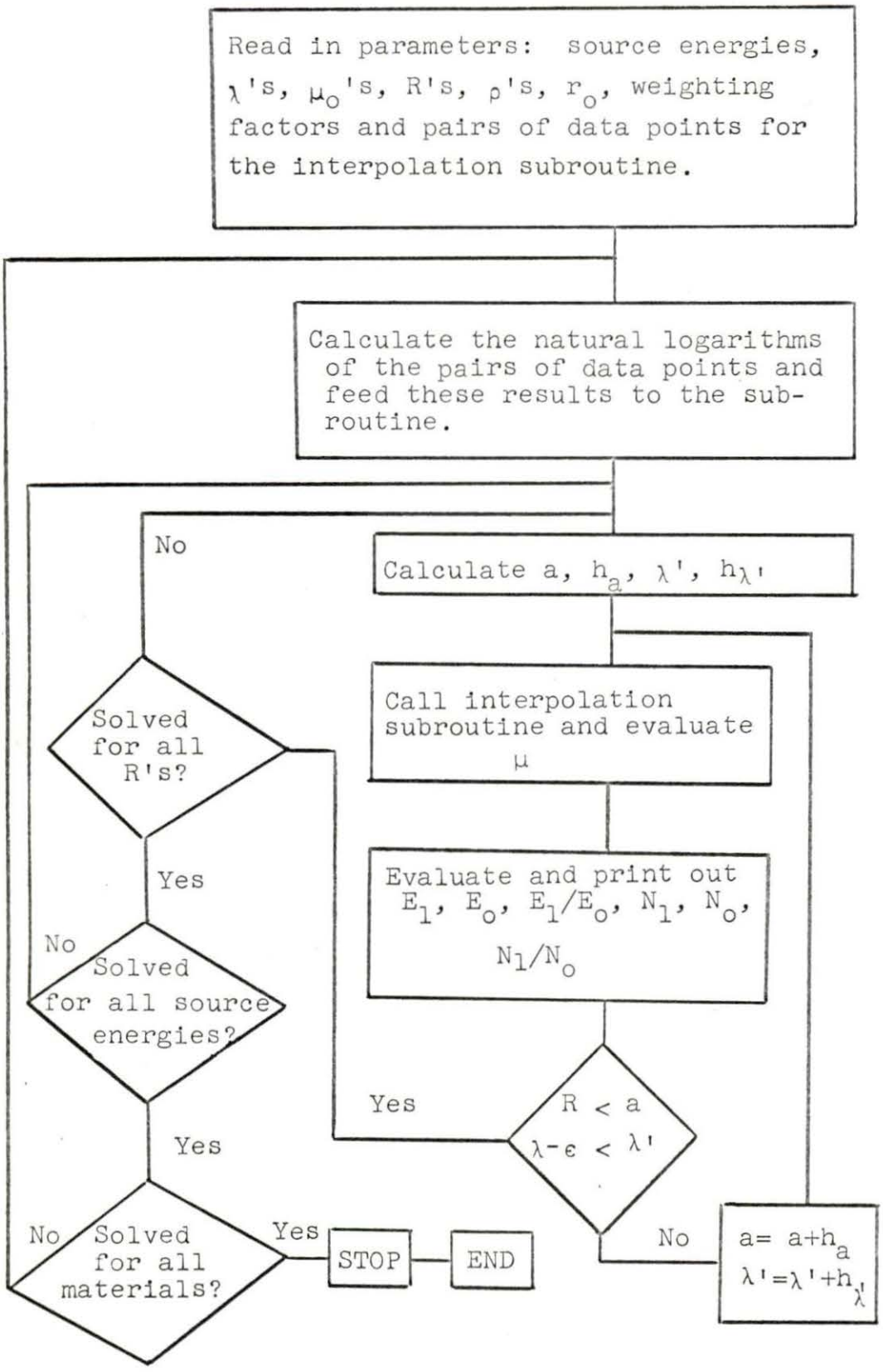
Read in parameters: source energies, λ's, μ_o's, R's, ρ's, r_o, weighting factors and pairs of data points for the interpolation subroutine.
Calculate the natural logarithms of the pairs of data points and feed these results to the subroutine.
Calculate a, h_a, λ', h_λ'
Call interpolation subroutine and evaluate μ
Evaluate and print out E_1, E_o, E_1/E_o, N_1, N_o, N_1/N_o
R < a
λ-ε < λ'
Yes
No
a= a+h_a
λ'=λ'+h_λ'
Solved for all R's?
No
Yes
Solved for all source energies?
No
Yes
Solved for all materials?
No
Yes
STOP
END

Figure 18. Flow diagram of the Lagrange's interpolation subroutine.

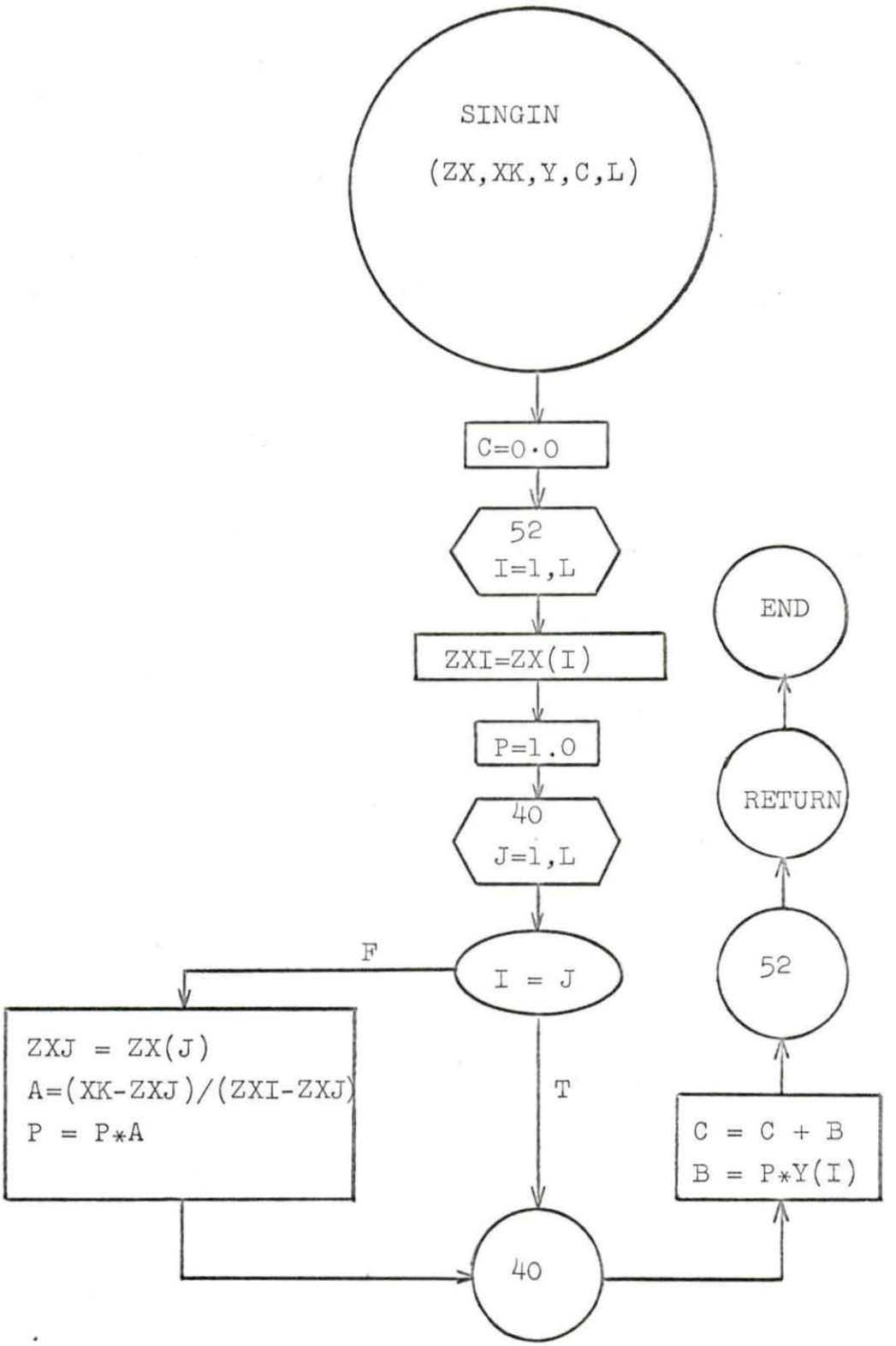
SINGIN
(ZX,XK,Y,C,L)
C=0.0
52
I=1,L
ZXI=ZX(I)
P=1.0
40
J=1,L
I = J
F
T
ZXJ = ZX(J)
A=(XK-ZXJ)/(ZXI-ZXJ)
P = P*A
40
C = C + B
B = P*Y(I)
52
RETURN
END